

THS

LIBRARIES MICHIGAN STATE UNIVERSITY EAST LANSING, MICH 48824-1048

62195793

This is to certify that the thesis entitled

THE USE OF LASER ABLATION INDUCTIVELY COUPLED PLASMA MASS SPECTROMETRY (LA-ICP-MS) FOR THE DISCRIMINATION OF GLASS FRAGMENTS IN FORENSIC CASEWORK

presented by

David William Szymanski

has been accepted towards fulfillment of the requirements for the

M.S. degree in Forensic Chemistry

Major Professor's Signature

11/11/04

Date

MSU is an Affirmative Action/Equal Opportunity Institution

PLACE IN RETURN BOX to remove this checkout from your record. TO AVOID FINES return on or before date due. MAY BE RECALLED with earlier due date if requested.

	<u>DATE DUE</u>	<u>DATE DUE</u>	DATE DUE
	MAY 1 6 2007		
Α	PR 1 8 2007		
	V		

6/01 c:/CIRC/DateDue.p65-p.15

THE USE OF LASER ABLATION INDUCTIVELY COUPLED PLASMA MASS SPECTROMETRY (LA-ICP-MS) FOR THE DISCRIMINATION OF GLASS FRAGMENTS IN FORENSIC CASEWORK

By

David William Szymanski

A THESIS

Submitted to
Michigan State University
In partial fulfillment of the requirements
For the degree of

Master of Science in Forensic Chemistry

School of Criminal Justice

2004

ABSTRACT

THE USE OF LASER ABLATION INDUCTIVELY COUPLED PLASMA MASS SPECTROMETRY (LA-ICP-MS) FOR THE DISCRIMINATION OF GLASS FRAGMENTS IN FORENSIC CASEWORK

By

David William Szymanski

Inductively coupled plasma mass spectrometry (ICP-MS) is becoming a widely used method for elemental analyses of glass fragments, with laser ablation (LA) of solid samples being the most efficient introduction system for forensic applications (e.g. Trejos et al., 2003). Trace element abundances in glasses are widely variable, even in glasses of the same refractive index. This variability allows for a high degree of discrimination when comparing ratios of trace element abundances. Laser ablation requires little or no sample preparation, which reduces opportunity for contamination, and is virtually nondestructive. In order to use the technique for routine forensic analyses of glass fragments in casework, it was necessary to test the precision of the technique and the homogeneity of samples to avoid erroneous interpretations of the results. A protocol for the analysis of glass fragments by LA-ICP-MS was developed using a set of ten "unknown" automobile float glass fragments and a National Institute of Standards and Technology glass. A graphical technique was employed for comparing element ratios in samples, based on the work of Watling et al. (1997). After confirming the homogeneity of glass samples and ensuring reproducibility of individual analyses, the technique was applied to casework for the Michigan State Police. When samples cannot be distinguished by physical parameters such as refractive index, they are analyzed by LA-ICP-MS. Three cases are presented as examples of the discriminatory and associative power of the method.

For Jack Brownstein.

ACKNOWLEDGEMENTS

This research was accomplished with the support of many colleagues, friends and members of my family. Jay Siegel, Lina Patino, Christopher Bommarito, and Thomas Vogel served as advisors throughout the project, offering numerous discussions, critiques, and ideas to help me transfer the research into practical application. Christopher Smith is thanked for his role as a reader from the School of Criminal Justice. Special thanks are offered to Lina Patino for her patient, comprehensive teaching of ICP-MS techniques and data interpretation. Likewise, the friendship and exceptional instruction of Christopher Bommarito fueled my interest in glass and encouraged my pursuit of excellence in criminalistics. I am grateful that the Department of Geological Sciences and School of Criminal Justice at Michigan State University allowed me to pursue dual degrees and supported my interdisciplinary approach to learning and teaching. The result here is a cooperative program that involves both departments and the Michigan State Police, working together to solve real-world problems through science. Accordingly, I must thank the Michigan State Police and detectives throughout Michigan for their help in completing this research.

The loves of my life, Anne and Hannah, serve as a constant reminder of why all of this matters. Likewise, my parents, brother, sisters, and extended family are a source of endless support and joy in my life. I would also like to thank numerous friends from Michigan and Minnesota for encouraging me.

TABLE OF CONTENTS

LIST OF TABLES	vi
LIST OF FIGURES	vii
INTRODUCTION	1
EXPERIMENTAL SETUP	
Instrumentation and Materials	
Experimental Design	5
RESULTS AND DISCUSSION	8
Precision and Discrimination	18
Precision and Sample Homogeneity	29
APPLICATION OF THE METHOD: CASEWORK EXAMPLES	31
Case #1: Lansing, MI Homicide	34
Case #2: Saginaw, MI Homicide	34
Case #3: Dundee, MI Breaking and Entering	36
CONCLUSIONS AND FUTURE WORK	36
REFERENCES	41

LIST OF TABLES

Table 1. List of ten samples treated as unknowns in this study and sample codes use text	
Table 2. Integrated peak heights for all analyses. (n/a = not acquired)	9
Table 3. Sr-normalized peak heights for analyses	14
Table 4. Precision RSD values for non-float and float side analyses for all sample Phase I and II. Each RSD value includes five replicate analyses on the non-float and five analyses on the float side of each fragment. RSD values are given for pheights normalized to Sr.	side peak
Table 5. Precision RSD values for analyses in two cross-sectional traverses in Phasand II. RSD values are given for peak heights normalized to Sr	

LIST OF FIGURES

Figure 1. Plot of all analyses for the set of six unknown fragments and NIST 612 from Phase I. Symbols represent five replicate analyses for each sample on the non-float side of fragments. Note that only two samples, 89GrandAm and 93Cav, are not clearly differentiated using these three elements (Zr-La-Ba)
Figure 2. Plot of all analyses for the set of six unknown fragments and NIST 612 from Phase I, replacing La in Figure 1 with Sr at the top apex. Symbols are the same as Figure 1. Notice that all samples, including 89GrandAm and 93Cav from Figure 1 are clearly separated
Figure 3. Plot of all analyses for the set of six unknown fragments and NIST 612 from Phase II. Symbols represent five replicate analyses for each sample on the float side of fragments
Figure 4. Plot of all analyses for the set of six unknown fragments and NIST 612 from both Phase I and Phase II. Closed symbols represent five replicate analyses for each sample on the non-float side of fragments (Phase I) while open symbols represent five replicate analyses on the float side of fragments (Phase II)
Figure 5. Plot of all analyses for the set of additional four unknown fragments and NIST 612 from Phase III. Symbols represent ten replicate analyses for each sample, five replicates on the non-float side and five replicates on the float side of fragments. Note that the fragments that are not clearly discriminated in the plot (Sr-Y-Zr) can be differentiated using an additional three elements (Ce-Ba-La, inset)
Figure 6. Plot of all analyses for the set of additional four unknown fragments and NIST 612 from Phase III showing the effect of multiplying one component (Y) by a factor of ten. Symbols are the same as Figure 5
Figure 7. Plot of all analyses for the entire set of ten unknown fragments and NIST 612 from Phase I, II, and III. Symbols represent ten replicate analyses for each sample, five replicates on the non-float side and five replicates on the float side of fragments. See text for discussion of samples 90Accord and 90Sunbird, which cannot be graphically discriminated using any combination of elements
Figure 8. Schematic diagrams of cross-sectional traverses of sample 86LabGTS from Phase II. Analyses were spaced 300 µm apart for a total of 13 ablation points. A. Plot of distance versus peak height (counts) for Ce and Y along the cross-section. B. Plot of distance versus peaks heights for Ce and Y normalized to Sr. Note the relatively flat profiles using normalized values

LIST OF FIGURES, CONTINUED

Figure 9. Schematic diagrams of cross-sectional traverses of sample 94Metro from Phase III. Analyses were spaced 300 μm apart for a total of seven ablation points. A. Plot of distance versus peak height (counts) for La and Ba along the cross-section. B. Plot of distance versus peaks heights for La and Ba normalized to Sr. Again, note the relative flat profiles using normalized values
Figure 10. Plot showing one of the diagrams used to conclude that the questioned and known fragments in the homicide case could have originated from the same source. Each sample was analyzed three times. Combinations of other elements produced the same results; none of the fragments could be discriminated
Figure 11. Plot showing one of the diagrams used to conclude that the questioned fragment from the front porch and the known fragment from the south window could have originated from the same source. Note that the questioned fragment from the hammer handle is easily excluded as coming from the same source as the other two fragments. Again, each sample was analyzed three times
Figure 12. Plot showing one of the diagrams used to conclude that the questioned fragment from the suspect's shoe and the known fragment from the convenience store window did not originate from the same source. As in previous cases, each sample was analyzed three times

INTRODUCTION

Glass is used universally in packaging, architecture, and motor vehicles. Float glass, named for the process by which molten glass is cooled and thinned as it is floated atop a layer of liquid tin, defines an important and frequently encountered type of glass evidence. Commonly used in architectural and automotive windows, float glass is easily dispersed and transferred during the commission of crimes. With the increasing physical and chemical homogeneity of float glass, forensic scientists must use innovative techniques to strengthen associations and add discriminating power to analytical schemes that rely upon traditional optical techniques, such as the determination of refractive index.

In the absence of a physical match, forensic scientists typically classify glass fragments according to their physical properties of color, thickness (when parallel sides are present), and refractive index. When exclusions cannot be made based on these properties, elemental analyses can provide crucial additional information for classification and discrimination of fragments (Hickman, 1987). Major element variation in glass is often associated with changes in refractive index (Parouchais et al., 1996). Trace elements, however, are more variable, even among glasses with analytically indistinguishable refractive indexes (e.g. Duckworth et al., 2002). For this reason, it has been clearly demonstrated in pairwise comparison studies that while refractive index measurements alone can discriminate roughly 40-50% of different glasses in large sample sets (e.g. 40-70 sample samples, or roughly 1000-2500 pairs), the addition of trace element data decreases the number of indistinguishable pairs to 0-5%, depending on the rigor of the statistical comparison (Trejos et al., 2003; Duckworth et al., 2002).

Inductively coupled plasma mass spectrometry (ICP-MS), with multielement capabilities, low detection limits, and a dynamic range that normally spans eight orders of magnitude, is well suited for trace element analyses of glass fragments. The use of ICP-MS for elemental analysis of glass is well documented by solution nebulization of acid-digested fragments (e.g. Parouchais et al., 1996; Suzuki et al., 2000; Duckworth et al., 2000; Duckworth et al., 2002; Trejos et al., 2003; Montero et al., 2003) and by laser ablation (e.g. Watling et al., 1997; Watling, 1999; Trejos et al., 2003; Trejos and Almirall, 2004). In the case of solution nebulization, fragments are first dissolved in an acid cocktail consisting of two or more of the following acids in varying proportions: hydrofluoric (HF), nitric (HNO₃), hydrochloric (HCl) and/or perchloric (HClO₄). The solutions are then aspirated through a small annulus and carried to the plasma in liquid aerosol form.

During laser ablation of glass, radiation from the laser couples with the sample and produces intense heat at its surface. The sample is partially melted and vaporized, with some of the material being quenched into microscopic glass beads. The solid particles are subsequently swept away by an inert carrier gas to be atomized, then ionized by the plasma and sent to a mass spectrometer. Elemental fractionation, whereby the composition of the material analyzed is not representative of the material being ablated, can occur due to a combination of factors, including but not limited to: depth and morphology of the crater produced by ablation, laser beam properties, transport of various particle sizes, and sample matrix effects (Russo et al., 2002). However, in a recent study using glass standards and float glass samples, Trejos and Almirall (2004)

found that most elements show low levels of fractionation during ablation and fractionation does not appreciably affect elemental comparisons in forensic casework.

As reviewed by Durrant (1999) and Russo et al. (2002), laser ablation has been used in a wide variety of geological, biological, materials science, and forensic applications. Depending on the sample and ablation parameters, as little as microgram (10⁻⁶ g), nanogram (10⁻⁹ g), or even femtogram (10⁻¹⁵ g) quantities may suffice for an analysis (Russo et al., 2002). Glass fragments submitted to the forensic scientist are often microscopic; the small volume of material required for LA-ICP-MS makes the method almost non-destructive even for the smallest fragments. The lack of sample preparation minimizes opportunity for contamination of samples and significantly reduces analysis time. The efficiency of LA-ICP-MS makes it ideally suited for forensic elemental analysis of glass fragments.

Although true quantification of elemental abundances in glass samples is not possible without the use of other techniques to determine the concentration of at least one element to be used as an internal standard, the use of elemental ratios has been demonstrated to be a precise and effective discriminating tool for comparisons, even when using solution nebulization. Parouchais et al. (1996) note that in cases where acid-digested fragments are too small to be accurately massed for quantification, elemental ratios are well suited for sample comparison. Watling et al. (1997) suggested the use of ternary discrimination diagrams for comparing trace element ratios in samples. Such diagrams (see below, Figure 1) allow for fast graphical discrimination of samples based on a number of different combinations of elements.

This research took a two-fold approach to overcome several roadblocks to LA-ICP-MS analysis of forensic glass samples. The first goal was to develop a protocol for the ablation of glass fragments in the ICP-MS laboratory at Michigan State University and determine the precision of the technique for the standard reference glass from the National Institute of Standards and Technology (NIST 612) and a set of automobile float glass samples collected by the Michigan State Police. In order to use the technique for casework, it was necessary to demonstrate that the analyses are precise, regardless of which part of a fragment is sampled. As float glass is produced, tin (Sn) is imparted to a very thin (µm-order) portion of the "float" side of the glass, the side in contact with the liquid tin. A clear concern, therefore, was whether trace elements were heterogeneously distributed throughout a fragment, which would lead to imprecise analyses and possibly erroneous exclusions in comparisons.

The second goal was to develop a method for efficiently evaluating the data, discriminating between samples using trace element ratios in actual casework. As described above, much work is being done to develop the method in terms of optimizing discrimination power of the technique (e.g. Trejos et al., 2003) and in the statistical comparison of sample sets (e.g. Aeschliman et al, 2004; Koons and Buscaglia, 2002; Koons and Buscaglia, 1999; Curran et al., 1997a, 1997b). The purpose of this study was to employ the laser ablation technique for discrimination in actual casework. The method was designed to compliment comparison techniques currently employed by the Michigan State Police, including refractive index determination by the Emmons double-variation method and scanning electron microscopy energy-dispersive spectroscopy (SEM-EDS) for major element composition.

EXPERIMENTAL SETUP

Instrumentation and Materials

A CETAC LSX-200® Plus Q switched Nd:YAG laser (266 nm) attached to a Micromass Platform® ICP-MS, a quadrupole mass spectrometer, was used in all experiments. The Platform features and in-line hexapole collision cell, which reduces elemental interferences with the argon carrier gas (e.g. ⁴⁰Ar¹⁶O⁺ on ⁵⁶Fe). The LSX laser focus ranges from a 10-250 μm beam diameter and has precision translation stage movement (x, y and z) within 0.25 μm. NIST 612, a glass standard with ~50 ppm concentrations of the trace elements that is used for tuning the instrument, was incorporated as a known standard for precision in all experiments. Ten sets of automobile float glass fragments were provided by the Michigan State Police Forensic Science Division. Fragments were collected by the Michigan State Police and represent ten models from seven manufacturers (Table 1). All unknown samples had parallel sides; the side of each fragment in contact with the liquid tin during production, the "float side," was identified by UV fluorescence and labeled with permanent maker.

Experimental Design

In the first phase of the project, a protocol for ablation of NIST 612 and one "unknown" glass fragment was developed. Based on previous glass discrimination studies by Parouchais et al. (1996), Watling et al (1997), Becker (2000), and Duckworth et al. (2002), a menu of eight isotopes was selected for data acquisition by LA-ICP-MS. A scan of these eight isotopes (85Rb, 88Sr, 89Y, 90Zr, 98Mo, 138Ba, 139La, and 140Ce) was

Year	Manufacturer Model	Model	Sample Code
1990	Honda	Accord	90Accord
1989	Pontiac	Grand Am	89GrandAm
1995	Ford	Contour	95Cont
1986	Chysler	Lebaron GTS	86LabGTS
1993	Chevrolet	Cavalier	93Cav
1990	Chevrolet	Beretta	90Beretta
1990	Pontiac	Sunbird	90Sunbird
1985	Oldsmobile	Brougham	89Brougham
1989	Plymouth	Sundance	89Sundance
1994	Geo	Metro	94Metro

Table 1. List of ten samples treated as unknowns in this study and sample codes used in text.

conducted for 60 s in each trial of protocol development, during which the transient signal was acquired by the detector. Ablation parameters were optimized in depth-profile ablation mode, using both NIST 612 and 1993 Chevrolet Cavalier (93Cav, see Table 1). Variables optimized included: spot size, rate of penetration into sample by raising the sample stage (z-rate), and duration of ablation. In each trial, a 1 s pre-ablation burst of the laser at the sample surface was conducted (100% energy output) to eliminate any possible contamination. In each trial, the pre-ablation spot size was 100 µm larger in diameter than the ablation spot size. The 60 s scan was initiated before ablation began and continued after ablation was complete, making it possible to easily identify any welldefined transient peaks above background, with a 0.1 s dwell time for each isotope. The technique was optimized for the smallest spot size (best for forensic applications) that produced adequate signal above background. For both NIST 612 and the unknown sample, this condition was met using a z-rate of 1 µm/s for 30 s and an ablation spot size of 100 µm. (The pre-ablation laser burst for contamination prevention was consequently set with a spot size of 200 µm.)

Using this protocol, NIST 612 and a set of the samples from the Michigan State Police (n=10) were ablated to test 1.) the precision of the technique and 2.) sample homogeneity. In this first phase, a subset of samples (n=6) was analyzed, including: 93Cav, 89GrandAm, 86LabGTS, 95Cont, 90Beretta, and 90Accord. The non-float side of each sample was ablated five times, with each ablation spaced 500 µm away from the preceding point. In the second phase of experiments, eight months later, the float side of each unknown sample was ablated in the same manner to ascertain the degree of homogeneity of the samples between the float and non-float sides. In the third phase,

another subset of samples (n=4) was ablated using the same parameters seven months later to expand the data set for comparison. From Table 1, these samples included: 94Metro, 90Sunbird, 89Sundance, and 89Brougham. Samples were similarly ablated five times on both the float and non-float sides of the samples. In addition, a cross-sectional traverse of two samples was performed during Phase II (86LabGTS) and Phase III (94Metro) of the experiments. In addition to testing reproducibility of measurements, the purpose of these trials was to ensure homogeneity of the samples when no parallel sides are present, as is often the case when glass samples are submitted to analysts in casework.

RESULTS AND DISCUSSION

All data were reduced using the MassLynx software provided by the ICP-MS manufacturer (Micromass, Ltd., Manchester, England), which performs a standard guassian integration of peaks, yielding a maximum peak height for each isotope (Table 2). As precision in this study is determined by measurements of element ratios, relative standard deviation (RSD) is considered for peak heights normalized to ⁸⁸Sr (Table 3). Data are presented in chronological order by groups of analyses (Phases I, II, and III).

Overall, precision for sets of replicate analyses is good, with RSD values of <10% for most elements, many <5% (Table 3). In the first two phases of research, ⁸⁵Rb and ⁹⁸Mo, which had the lowest peak heights of all isotopes, were the only two elements to demonstrate precision consistently >10% RSD. In all subsequent analyses, ⁸⁵Rb and ⁹⁸Mo were removed from the element menu. In rare cases, for the other elements in the menu (⁸⁸Sr, ⁸⁹Y, ⁹⁰Zr, ¹³⁸Ba, ¹³⁹La, and ¹⁴⁰Ce), precision RSD values exceed >10%. For example, ¹³⁹La for 90Sunbird has a precision RSD of 29.7% (Table 3). However, the

Table 2. Integrated peak heights for all analyses. (n/a = not acquired)

Sample/replicate	Type of analysis				Peak Height (counts	it (counts)			
		Rb	Sr	>	Zr	Μo	Ba	La	రి
PHASE I									
NIST 612-1	Standard	222818	386718	168672	86477	81853	232802	225109	319506
NIST 612-2	Standard	180095	329124	139183	70631	66405	195220	194788	278830
NIST 612-3	Standard	167880	292487	126394	64749	86979	166765	171301	240269
NIST 612-4	Standard	197802	343883	152539	78290	68370	201028	206872	277204
NIST 612-5	Standard	182753	322236	143193	73008	65055	192518	194469	261359
93Cav-1	Non-float side	16748	329621	16945	411409	2398	104077	15475	90490
93Cav-2	Non-float side	11458	335704	16913	391909	2684	93754	15467	85092
93Cav-3	Non-float side	9287	278850	14634	333561	1983	78792	13031	75192
93Cav-4	Non-float side	41142	313321	15728	378464	2331	94572	15017	86122
93Cav-5	Non-float side	8252	312945	16458	375363	2518	90844	14233	83459
89GrandAm-1	Non-float side	19242	759226	22839	562525	3841	153840	18690	47609
89GrandAm-2	Non-float side	16679	715275	24031	547443	3004	146220	18248	45319
89GrandAm-3	Non-float side	16144	668280	22702	525160	2857	133379	17512	41406
89GrandAm-4	Non-float side	15022	670372	22117	519661	2501	136551	17382	42244
89GrandAm-5	Non-float side	16732	668166	21798	518779	2582	134667	17119	41531
86LabGTS-1	Non-float side	348105	324029	33765	316380	2865	799927	52300	142360
86LabGTS-2	Non-float side	326846	313393	31218	292190	3680	757461	49505	133828
86LabGTS-3	Non-float side	330359	315190	32333	300927	2615	752153	49412	134278
86LabGTS-4	Non-float side	328529	301155	30539	294568	2043	736267	49436	135192
86LabGTS-5	Non-float side	304098	286523	29790	287342	2150	708524	45931	122518
95Cont-1	Non-float side	27295	531354	48256	1941725	4917	141110	24341	00629
95Cont-2	Non-float side	22658	516320	46747	1827062	4440	131551	23911	64121
95Cont-3	Non-float side	17331	497265	45891	1803388	3989	129011	22410	62846
95Cont-4	Non-float side	22477	563498	51829	2045082	4433	143747	26222	71019
95Cont-5	Non-float side	13604	497137	45953	1775585	3877	125559	23422	61803
90Beretta-1	Non-float side	16053	352926	9689	72093	3937	100815	23001	65894
90Beretta-2	Non-float side	21772	347014	5598	68751	3215	91989	21444	61976
90Beretta-3	Non-float side	17436	319560	5799	65913	2188	89797	20869	62345
90Beretta-4	Non-float side	15816	334722	5940	65554	2257	84594	20866	57423

Table 2, continued. Integrated peak heights for all analyses. $(n/a = not \ acquired)$

Sample/replicate	Type of analysis	į	ı	;	Peak Height (counts)	t (counts)	(,	(
		Rb	Sr	> ;	Zr	Wo	Ba	ra S	ဗီ
	Non-float side	16077	323317	5749	62156	1897	82455	20615	58410
	Non-float side	33409	714441	15848	261515	4750	201112	24424	71835
	Non-float side	24152	592719	13508	223585	3022	146335	20338	58177
	Non-float side	21205	699695	12695	214334	2051	144845	20396	57562
	Non-float side	26491	608193	14327	234227	2440	172653	21048	60010
	Non-float side	21422	553981	13066	209868	2223	143765	18729	54265
	Standard	248793	438217	182671	91796	84459	233177	247395	311656
	Standard	250829	455974	193460	99354	94778	245756	257882	324118
	Standard	261060	410920	173185	86024	93582	219981	219847	286355
	Standard	195987	343056	149080	73427	95569	185136	194171	245160
	Standard	293480	443587	190681	92876	99170	235322	237569	315509
	Float side	71484	727716	33903	768424	15960	242410	33151	195436
	Float side	34200	636744	32786	696055	10586	179968	29050	169667
	Float side	40188	589730	29635	665603	7699	166807	26949	157658
	Float side	25029	611830	29622	678929	6517	170471	26888	151646
	Float side	23514	582766	29207	648332	4500	170450	25135	146984
	Float side	49610	1357440	43353	974348	14743	295730	35816	99906
	Float side	58662	1184676	38388	881051	10689	250515	30729	67335
	Float side	50942	1196158	36823	858189	9480	239273	29976	72210
	Float side	39756	1071176	34855	781514	5782	212981	27668	65048
	Float side	30830	1120491	36314	833276	7182	230749	28000	64781
	Float side	612896	809085	55536	488101	12719	1226116	81805	215042
	Float side	587343	529896	51014	467785	6246	1191429	81741	203889
	Float side	538304	487939	49636	437982	6927	1098518	72284	187320
	Float side	552409	491630	48942	436946	6234	1126008	75478	192679
	Float side	548285	501403	49905	469490	4960	1165978	77924	194383
	Float side	54375	995439	86567	3197412	11821	296558	43892	121607
	Float side	43361	875084	79179	2825999	16182	234482	38612	10001

Table 2, continued. Integrated peak heights for all analyses. $(n/a = not \ acquired)$

Sample/replicate	Type of analysis				Peak Height (counts)	t (counts)			
		Rb	Sr		Zr	Mo	Ba	La	ප
95Cont-3	Float side	33719	827704	73039	2651593	7999	222929	35583	93252
95Cont-4	Float side	26873	837817		2766188	7733	218901	36068	93474
95Cont-5	Float side	55057	795697		2574769	5063	206837	35270	97131
90Beretta-1	Float side	36479	571131		119158	4 04	158263	34103	87954
90Beretta-2	Float side	39040	560935		115006	5074	141100	33928	85754
90Beretta-3	Float side	25282	554669		114681	4303	137427	33364	84217
90Beretta-4	Float side	29437	533681		109819	4655	141488	33086	81863
90Beretta-5	Float side	22776	505862		105444	4994	147428	31540	76048
90Accord-1	Float side	75081	1097295		402878	11371	294329	36305	99385
90Accord-2	Float side	52600	961453		356387	5946	242530	32383	84454
90Accord-3	Float side	45001	908025		353338	8753	233041	31368	78861
90Accord-4	Float side	53240	962402		358463	5674	242636	33456	92276
90Accord-5	Float side	48381	940550		349227	4692	219009	30357	79548
86Lab-X-top-1	Cross-section	1261958	1074872		851550	19706	2463718	150928	400047
86Lab-X-2	Cross-section	1209794	1059907		841849	13336	2375629	146986	394686
86Lab-X-3	Cross-section	957941	839727		665947	10622	1834720	118157	315135
86Lab-X-4	Cross-section	964748	803002		660935	9096	1862374	116101	309000
86Lab-X-5	Cross-section	980573	828818		667289	7590	1911226	120530	319569
86Lab-X-6	Cross-section	922310	768088		640391	6154	1786085	111045	298665
86Lab-X-7	Cross-section	1247105	1004343		805974	8581	2199729	136584	383730
86Lab-X-8	Cross-section	897170	768684		621950	5861	1759752	116074	297121
86Lab-X-9	Cross-section	901463	771902		643876	6682	1736336	109780	290893
86Lab-X-10	Cross-section	772472	090659		570272	7387	1535037	100304	263963
86Lab-X-11	Cross-section	1037420	821188		764182	7781	1875840	117341	320432
86Lab-X-12	Cross-section	938698	849532		757875	6295	2109676	136211	339084
86Lab-X-bottom-13	Cross-section	1106983	888190		764883	8911	2163248	141855	365286
PHASE III									
NIST 612-1	Standard	n/a	1044606	481819	241696	n/a	547145	627885	762650
NIST 612-2	Standard	n/a	1038006	477319	244016	n/a	559119	621475	752743

Table 2, continued. Integrated peak heights for all analyses. (n/a = not acquired)

Sample/replicate	Type of analysis				Peak Heigh	t (counts)			
		Rb	Sr		Zr	Mo	Ba	La	ප
NIST 612-3	Standard	n/a	953219	446996	222366	n/a	499693	551031	675625
NIST 612-4	Standard	n/a	914166		207549	n/a	477314	536232	642870
NIST 612-5	Standard	n/a	948302		219573	n/a	517315	565489	681754
85Brougham-1	Non-float side	n/a	1332897		1327407	n/a	346862	41277	101683
85Brougham-2	Non-float side	n/a	1417568		1388982	n/a	293596	40009	94661
85Brougham-3	Non-float side	n/a	1346948		1352184	n/a	281312	38075	81451
85Brougham-4	Non-float side	n/a	1312083		1325382	n/a	264855	34933	76331
85Brougham-5	Non-float side	n/a	1372276		1374545	n/a	280570	36131	80091
85Brougham-1	Float side	n/a	1573470		1736693	n/a	328751	44488	93095
85Brougham-2	Float side	n/a	1306918		1447076	n/a	375147	34780	81181
85Brougham-3	Float side	n/a	1517460		1696792	n/a	312759	40703	81608
85Brougham-4	Float side	n/a	1536548		1640376	n/a	313499	40886	86487
85Brougham-5	Float side	n/a	1497051		1656686	n/a	301846	38840	84815
89Sundance-1	Non-float side	n/a	1000305		767938	n/a	320007	73479	159205
89Sundance-2	Non-float side	n/a	941443		704213	n/a	265585	71529	141341
89Sundance-3	Non-float side	n/a	931639		733066	n/a	262134	66791	134125
89Sundance-4	Non-float side	n/a	915238		705592	n/a	251055	64946	130873
89Sundance-5	Non-float side	n/a	928916		707566	n/a	251552	65628	136011
89Sundance-1	Float side	n/a	1108910		816644	n/a	295860	73566	161708
89Sundance-2	Float side	n/a	992642		778346	n/a	267299	70445	141222
89Sundance-3	Float side	n/a	1036744		810982	n/a	276305	75797	153954
89Sundance-4	Float side	n/a	916154		736095	n/a	252178	65999	130746
89Sundance-5	Float side	n/a	1002168		770360	n/a	270498	72854	147871
94Metro-1	Non-float side	n/a	886921		611824	n/a	158216	39160	130517
94Metro-2	Non-float side	n/a	743682		520880	n/a	128977	33073	105711
94Мето-3	Non-float side	n/a	721571		497016	n/a	123268	32246	102657
94Metro-4	Non-float side	n/a	692501		490851	n/a	123196	31332	98399
94Metro-5	Non-float side	n/a	685751		488648	n/a	120327	30095	96855
94Metro-1	Float side	n/a	805452		525863	n/a	143397	36258	114014
94Меtro-2	Float side	n/a	776703		516930 n/a	n/a	131328	34086	107996

Table 2, continued. Integrated peak heights for all analyses. (n/a = not acquired)

Sample/replicate	Type of analysis				Peak Height (counts	t (counts)			
		Rb	Sr	¥	Zr	Mo	Ba	La	రి
94Метю-3	Float side	n/a	731190	26316	508558	n/a	129197	33230	102108
94Мето-4	Float side	n/a	737268	27090	492510	n/a	125840	30462	101519
94Metro-5	Float side	n/a	851485	28792	557717	n/a	149684	36633	120183
90Sunbird-1	Non-float side	n/a	1213171	30418	489431	n/a	285769	82311	112846
90Sunbird-2	Non-float side	n/a	1176247	30457	472772	n/a	257721	45362	101194
90Sunbird-3	Non-float side	n/a	1141017	29967	465273	n/a	260199	43996	100745
90Sunbird-4	Non-float side	n/a	1096645	28865	456573	n/a	253485	42201	95398
90Sunbird-5	Non-float side	n/a	1091088	28785	456030	n/a	246637	41454	94212
90Sunbird-1	Float side	n/a	1256393	30217	511708	n/a	296986	45078	105756
90Sunbird-2	Float side	n/a	1206620	32299	896005	n/a	267047	46769	102095
90Sunbird-3	Float side	n/a	1160973	28647	482324	n/a	256833	45567	100133
90Sunbird-4	Float side	n/a	1147604	30528	489920	n/a	256032	45054	96472
90Sunbird-5	Float side	n/a	1067234	27426	445160	n/a	228082	39270	89558
94Metro-X-top-1	Cross-section	n/a	1706535	57295	1001719	n/a	278394	67874	223104
94Metro-X-2	Cross-section	n/a	1369487	50314	877296	n/a	234128	56541	169227
94Metro-X-3	Cross-section	n/a	1553812	51171	892729	n/a	248153	60643	208999
94Metro-X-4	Cross-section	n/a	1326248	45691	848854	n/a	230310	57011	177931
94Metro-X-5	Cross-section	n/a	1270285	43151	799903	n/a	213874	54731	166884
94Metro-X-6	Cross-section	n/a	1546616	56022	1036195	n/a	283179	68155	214022
94Metro-X-bottom-7	Cross-section	n/a	1316805	48241	882071	n/a	220480	57243	180336

 Table 3. Sr-normalized Peak Heights for analyses.

PHASE I

IHASEI	San	nnle and neak	Sr for each re	nlicate (n=5)	D	SD %
	NIST 612	apie and peak	or for each rep	piicate (n=3)		3D /6
Rb	0.57618	0.54719	0.57397	0.57520	0.56714	2.1%
Y	0.43616	0.42289	0.43214	0.44358	0.44437	2.0%
Zr	0.22362	0.21460	0.22137	0.22766	0.22657	2.3%
Mo	0.21166	0.20176	0.19481	0.19882	0.20189	3.1%
Ba	0.60199	0.59315	0.57016	0.58458	0.59744	2.1%
La	0.58210	0.59184	0.58567	0.60158	0.60350	1.6%
Ce	0.82620	0.84719	0.82147	0.80610	0.81108	1.9%
	93Cav					
Rb	0.05081	0.03413	0.03330	0.13131	0.02637	78.8%
Y	0.05141	0.05038	0.05248	0.05020	0.05259	2.2%
Zr	1.24813	1.16742	1.19620	1.20791	1.19945	2.4%
Mo	0.00728	0.00800	0.00711	0.00744	0.00805	5 .6%
Ba	0.31575	0.27928	0.28256	0.30184	0.29029	5.1%
La	0.04695	0.04607	0.04673	0.04793	0.04548	2.0%
Ce	0.27453	0.25347	0.26965	0.27487	0.26669	3.3%
	89GrandAm					
Rb	0.02534	0.02332	0.02416	0.02241	0.02504	5.0%
Y	0.03008	0.03360	0.03397	0.03299	0.03262	4.7%
Zr	0.74092	0.76536	0.78584	0.77518	0.77642	2.2%
Mo	0.00506	0.00420	0.00428	0.00373	0.00386	12.3%
Ba	0.20263	0.20442	0.19959	0.20369	0.20155	0.9%
La	0.02462	0.02551	0.02620	0.02593	0.02562	2.4%
Се	0.06271	0.06336	0.06196	0.06302	0.06216	0.9%
	86LabGTS					
Rb	1.07430	1.04293	1.04813	1.09090	1.06134	1.8%
Y	0.10420	0.09961	0.10258	0.10141	0.10397	1.9%
Zr	0.97639	0.93234	0.95475	0.97813	1.00286	2.7%
Mo	0.00884	0.01174	0.00830	0.00678	0.00750	22.1%
Ba	2.46869	2.41697	2.38635	2.44481	2.47283	1.5%
La	0.16141	0.15796	0.15677	0.16415	0.16030	1.8%
Ce	0.43934	0.42703	0.42602	0.44891	0.42760	2.3%
		0112100	01.12002		3233	2.070
	95Cont					
Rb	0.05137	0.04388	0.03485	0.03989	0.02736	23.0%
Mo	0.00925	0.00860	0.00802	0.00787	0.00780	7.4%
Ba	0.26557	0.25479	0.25944	0.25510	0.25256	2.0%
La	0.04581	0.04631	0.04507	0.04653	0.04711	1.7%
Zr	3.65430	3.53862	3.62661	3.62926	3.57162	1.3%
Ce	0.12779	0.12419	0.12638	0.12603	0.12432	1.2%
Y	0.09082	0.09054	0.09229	0.09198	0.09244	1.0%

Table 3, continued. Sr-normalized Peak Heights for analyses.

Solution Solution
Y 0.01812 0.01613 0.01815 0.01775 0.01778 4.7% Zr 0.20427 0.19812 0.20626 0.19585 0.19224 2.9% Mo 0.01116 0.00926 0.00685 0.00674 0.00587 27.3% Mo 0.06517 0.06180 0.06531 0.06234 0.06376 2.5% La 0.06517 0.017860 0.19510 0.17155 0.18066 4.9% Ce 0.18671 0.17860 0.19510 0.17155 0.18066 4.9% POAccord Rb 0.04676 0.04075 0.03722 0.04356 0.03867 9.3% Y 0.02218 0.02279 0.02228 0.02356 0.02359 2.9% Zr 0.36604 0.37722 0.37624 0.38512 0.37884 1.8% Mo 0.00665 0.00510 0.00360 0.00401 0.00401 26.4% Ba 0.28150 0.24689 0.25426 <
Zr 0.20427 0.19812 0.20626 0.19585 0.19224 2.9% Mo 0.01116 0.00926 0.00685 0.00674 0.00587 27.3% Ba 0.28565 0.26509 0.28100 0.25273 0.25503 5.6% La 0.06517 0.06180 0.06531 0.06234 0.06376 2.5% Ce 0.18671 0.17860 0.19510 0.17155 0.18066 4.9% POAccord Rb 0.04676 0.04075 0.03722 0.04356 0.02359 2.9% Y 0.02218 0.02279 0.02228 0.02356 0.02359 2.9% Zr 0.36604 0.37722 0.37624 0.38512 0.37884 1.8% Mo 0.00665 0.00510 0.00360 0.00401 0.00401 26.4% Ba 0.28150 0.24689 0.25426 0.28388 0.25951 6.3% Ce 0.10055 0.09815 0.10104 0.09867 </td
Mo 0.01116 0.00926 0.00685 0.00674 0.00587 27.3% Ba 0.28565 0.26509 0.28100 0.25273 0.25503 5.6% La 0.06517 0.06180 0.06531 0.06234 0.06376 2.5% Ce 0.18671 0.17860 0.19510 0.17155 0.18066 4.9% 90Accord Rb 0.04676 0.04075 0.03722 0.04356 0.03867 9.3% Y 0.02218 0.02279 0.02228 0.02356 0.02359 2.9% Mo 0.00665 0.00510 0.00360 0.00401 0.00441 0.00441 0.00441 0.00441 0.00441 0.00441 0.00441 0.00441 0.00441 0.00441 0.00441 0.00444 0.00444 0.00444 0.00444 0.00444 0.00444 0.00444 0.00444 0.00444 0.00444 0.00444 0.00444 0.00444 0.00444 0.00444 0.00444 0.00444 0.00444 0.00
Ba 0.28565 0.26509 0.28100 0.25273 0.25503 5.6% La 0.06517 0.06180 0.06531 0.06234 0.06376 2.5% Ce 0.18671 0.17860 0.19510 0.17155 0.18066 4.9% 90Accord Rb 0.04676 0.04075 0.03722 0.04356 0.03867 9.3% Y 0.02218 0.02279 0.02228 0.02356 0.02359 2.9% Zr 0.36604 0.37722 0.37624 0.38512 0.37884 1.8% Mo 0.00665 0.00510 0.00360 0.00401 0.00401 26.4% Ba 0.28150 0.24689 0.25426 0.28388 0.25951 6.3% La 0.03419 0.03431 0.03580 0.03461 0.03381 2.2% Ce 0.10055 0.09815 0.10104 0.09867 0.09795 1.4% Sample and peak/Sr for each replicate (n=5) RSD %
Ce
O.18671 O.17860 O.19510 O.17155 O.18066 4.9%
Phase Phas
Rb 0.04676 0.04075 0.03722 0.04356 0.03867 9.3% Y 0.02218 0.02279 0.02228 0.02356 0.02359 2.9% Zr 0.36604 0.37722 0.37624 0.38512 0.37884 1.8% Mo 0.00665 0.00510 0.00360 0.00401 0.00401 26.4% Ba 0.28150 0.24689 0.25426 0.28388 0.25951 6.3% La 0.03419 0.03431 0.03580 0.03461 0.03381 2.2% Ce 0.10055 0.09815 0.10104 0.09867 0.09795 1.4% Sample and peak/Sr for each replicate (n=5) RSD % NIST 612 Rb 0.56774 0.55009 0.63531 0.57130 0.66161 8.1% Y 0.41685 0.42428 0.42146 0.43456 0.42986 1.6% Zr 0.20948 0.21789 0.20934 0.21404 0.21614 1.8%
Rb 0.04676 0.04075 0.03722 0.04356 0.03867 9.3% Y 0.02218 0.02279 0.02228 0.02356 0.02359 2.9% Zr 0.36604 0.37722 0.37624 0.38512 0.37884 1.8% Mo 0.00665 0.00510 0.00360 0.00401 0.00401 26.4% Ba 0.28150 0.24689 0.25426 0.28388 0.25951 6.3% La 0.03419 0.03431 0.03580 0.03461 0.03381 2.2% Ce 0.10055 0.09815 0.10104 0.09867 0.09795 1.4% Sample and peak/Sr for each replicate (n=5) RSD % NIST 612 Rb 0.56774 0.55009 0.63531 0.57130 0.66161 8.1% Y 0.41685 0.42428 0.42146 0.43456 0.42986 1.6% Zr 0.20948 0.21789 0.20934 0.21404 0.21614 1.8%
Y 0.02218 0.02279 0.02228 0.02356 0.02359 2.9% Zr 0.36604 0.37722 0.37624 0.38512 0.37884 1.8% Mo 0.00665 0.00510 0.00360 0.00401 0.00401 26.4% Ba 0.28150 0.24689 0.25426 0.28388 0.25951 6.3% La 0.03419 0.03431 0.03580 0.03461 0.03381 2.2% Ce 0.10055 0.09815 0.10104 0.09867 0.09795 1.4% PHASE II Sample and peak/Sr for each replicate (n=5) RSD % RSD % NIST 612 Rb 0.56774 0.55009 0.63531 0.57130 0.66161 8.1% Y 0.41685 0.42428 0.42146 0.43456 0.42986 1.6% Zr 0.20948 0.21789 0.20934 0.21404 0.21614 1.8% Mo 0.19273 0.20786 0.22
Zr 0.36604 0.37722 0.37624 0.38512 0.37884 1.8% Mo 0.00665 0.00510 0.00360 0.00401 0.00401 26.4% Ba 0.28150 0.24689 0.25426 0.28388 0.25951 6.3% La 0.03419 0.03431 0.03580 0.03461 0.03381 2.2% Ce 0.10055 0.09815 0.10104 0.09867 0.09795 1.4% Sample and peak/Sr for each replicate (n=5) RSD % NIST 612 Rb 0.56774 0.55009 0.63531 0.57130 0.66161 8.1% Y 0.41685 0.42428 0.42146 0.43456 0.42986 1.6% Zr 0.20948 0.21789 0.20934 0.21404 0.21614 1.8% Mo 0.19273 0.20786 0.22774 0.20275 0.22356 6.9% Ba 0.53210 0.53897 0.53534 0.539967 0.53050 0.8%
Mo 0.00665 0.00510 0.00360 0.00401 0.00401 26.4% Ba 0.28150 0.24689 0.25426 0.28388 0.25951 6.3% La 0.03419 0.03431 0.03580 0.03461 0.03381 2.2% Ce 0.10055 0.09815 0.10104 0.09867 0.09795 1.4% Sample and peak/Sr for each replicate (n=5) RSD % NIST 612 Rb 0.56774 0.55009 0.63531 0.57130 0.66161 8.1% Y 0.41685 0.42428 0.42146 0.43456 0.42986 1.6% Zr 0.20948 0.21789 0.20934 0.21404 0.21614 1.8% Mo 0.19273 0.20786 0.22774 0.20275 0.22356 6.9% Ba 0.53210 0.53897 0.53534 0.53967 0.53050 0.8% Ce 0.71119 0.71083 0.69686 0.71464 0.71127 1.0%
Ba 0.28150 0.24689 0.25426 0.28388 0.25951 6.3% La 0.03419 0.03431 0.03580 0.03461 0.03381 2.2% Ce 0.10055 0.09815 0.10104 0.09867 0.09795 1.4% PHASE II Sample and peak/Sr for each replicate (n=5) RSD % NIST 612 Rb 0.56774 0.55009 0.63531 0.57130 0.66161 8.1% Y 0.41685 0.42428 0.42146 0.43456 0.42986 1.6% Zr 0.20948 0.21789 0.20934 0.21404 0.21614 1.8% Mo 0.19273 0.20786 0.22774 0.20275 0.22356 6.9% Ba 0.53210 0.53897 0.53534 0.53967 0.53050 0.8% Ce 0.71119 0.71083 0.69686 0.71464 0.71127 1.0% Y 0.04659
La 0.03419 0.03431 0.03580 0.03461 0.03381 2.2% Ce 0.10055 0.09815 0.10104 0.09867 0.09795 1.4% PHASE II Sample and peak/Sr for each replicate (n=5) RSD % NIST 612 Rb 0.56774 0.55009 0.63531 0.57130 0.66161 8.1% Y 0.41685 0.42428 0.42146 0.43456 0.42986 1.6% Zr 0.20948 0.21789 0.20934 0.21404 0.21614 1.8% Mo 0.19273 0.20786 0.22774 0.20275 0.22356 6.9% Ba 0.53210 0.53897 0.53534 0.53967 0.53050 0.8% La 0.56455 0.56556 0.53501 0.56600 0.53556 3.0% Y 0.09823 0.05371 0.06815 0.04091 0.04035 39.9% Y 0.04659 0.05149
Ce 0.10055 0.09815 0.10104 0.09867 0.09795 1.4% PHASE II Sample and peak/Sr for each replicate (n=5) RSD % NIST 612 Rb 0.56774 0.55009 0.63531 0.57130 0.66161 8.1% Y 0.41685 0.42428 0.42146 0.43456 0.42986 1.6% Zr 0.20948 0.21789 0.20934 0.21404 0.21614 1.8% Mo 0.19273 0.20786 0.22774 0.20275 0.22356 6.9% Ba 0.53210 0.53897 0.53534 0.53967 0.53050 0.8% La 0.56455 0.56556 0.53501 0.56600 0.53556 3.0% Ce 0.71119 0.71083 0.69686 0.71464 0.71127 1.0% P3Cav-float Rb 0.09823 0.05371 0.06815 0.04091 0.04035 39.9% Y 0.04659
PHASE II Sample and peak/Sr for each replicate (n=5) RSD %
NIST 612 Rb 0.56774 0.55009 0.63531 0.57130 0.66161 8.1% Y 0.41685 0.42428 0.42146 0.43456 0.42986 1.6% Zr 0.20948 0.21789 0.20934 0.21404 0.21614 1.8% Mo 0.19273 0.20786 0.22774 0.20275 0.22356 6.9% Ba 0.53210 0.53897 0.53534 0.53967 0.53050 0.8% La 0.56455 0.56556 0.53501 0.56600 0.53556 3.0% Ce 0.71119 0.71083 0.69686 0.71464 0.71127 1.0% Y 0.04659 0.05149 0.05025 0.04842 0.05012 3.9% Zr 1.05594 1.09315 1.12866 1.10967 1.11251 2.5% Mo 0.02193 0.01663 0.01306 0.01065 0.00772 39.3% Ba 0.33311 0.28264 0.28285 0.27862 0.29248 7.6% La 0.04555 0.04562 0.04570 0.04395 0.04313 2.6%
NIST 612 Rb 0.56774 0.55009 0.63531 0.57130 0.66161 8.1% Y 0.41685 0.42428 0.42146 0.43456 0.42986 1.6% Zr 0.20948 0.21789 0.20934 0.21404 0.21614 1.8% Mo 0.19273 0.20786 0.22774 0.20275 0.22356 6.9% Ba 0.53210 0.53897 0.53534 0.53967 0.53050 0.8% La 0.56455 0.56556 0.53501 0.56600 0.53556 3.0% Ce 0.71119 0.71083 0.69686 0.71464 0.71127 1.0% Y 0.04659 0.05149 0.05025 0.04842 0.05012 3.9% Zr 1.05594 1.09315 1.12866 1.10967 1.11251 2.5% Mo 0.02193 0.01663 0.01306 0.01065 0.00772 39.3% Ba 0.33311 0.28264 0.28285 0.27862 0.29248 7.6% La 0.04555 0.04562 0.04570 0.04395 0.04313 2.6%
NIST 612 NIST 612 Rb 0.56774 0.55009 0.63531 0.57130 0.66161 8.1% Y 0.41685 0.42428 0.42146 0.43456 0.42986 1.6% Zr 0.20948 0.21789 0.20934 0.21404 0.21614 1.8% Mo 0.19273 0.20786 0.22774 0.20275 0.22356 6.9% Ba 0.53210 0.53897 0.53534 0.53967 0.53050 0.8% La 0.56455 0.56556 0.53501 0.56600 0.53556 3.0% Ce 0.71119 0.71083 0.69686 0.71464 0.71127 1.0% 93Cav-float Rb 0.09823 0.05371 0.06815 0.04091 0.04035 39.9% Y 0.04659 0.05149 0.05025 0.04842 0.05012 3.9% Zr 1.05594 1.09315 1.12866 1.10967 1.11251 2.5% Mo 0.02193
Rb 0.56774 0.55009 0.63531 0.57130 0.66161 8.1% Y 0.41685 0.42428 0.42146 0.43456 0.42986 1.6% Zr 0.20948 0.21789 0.20934 0.21404 0.21614 1.8% Mo 0.19273 0.20786 0.22774 0.20275 0.22356 6.9% Ba 0.53210 0.53897 0.53534 0.53967 0.53050 0.8% La 0.56455 0.56556 0.53501 0.56600 0.53556 3.0% Ce 0.71119 0.71083 0.69686 0.71464 0.71127 1.0% 93Cav-float Rb 0.09823 0.05371 0.06815 0.04091 0.04035 39.9% Y 0.04659 0.05149 0.05025 0.04842 0.05012 3.9% Zr 1.05594 1.09315 1.12866 1.10967 1.11251 2.5% Mo 0.02193 0.01663 0.01306 0.01065 </td
Y 0.41685 0.42428 0.42146 0.43456 0.42986 1.6% Zr 0.20948 0.21789 0.20934 0.21404 0.21614 1.8% Mo 0.19273 0.20786 0.22774 0.20275 0.22356 6.9% Ba 0.53210 0.53897 0.53534 0.53967 0.53050 0.8% La 0.56455 0.56556 0.53501 0.56600 0.53556 3.0% Ce 0.71119 0.71083 0.69686 0.71464 0.71127 1.0% 93Cav-float Rb 0.09823 0.05371 0.06815 0.04091 0.04035 39.9% Y 0.04659 0.05149 0.05025 0.04842 0.05012 3.9% Zr 1.05594 1.09315 1.12866 1.10967 1.11251 2.5% Mo 0.02193 0.01663 0.01306 0.01065 0.00772 39.3% Ba 0.33311 0.28264 0.28285 0.27862 0.29248 7.6% La 0.04555 0.04562 0
Zr 0.20948 0.21789 0.20934 0.21404 0.21614 1.8% Mo 0.19273 0.20786 0.22774 0.20275 0.22356 6.9% Ba 0.53210 0.53897 0.53534 0.53967 0.53050 0.8% La 0.56455 0.56556 0.53501 0.56600 0.53556 3.0% Ce 0.71119 0.71083 0.69686 0.71464 0.71127 1.0% 93Cav-float Rb 0.09823 0.05371 0.06815 0.04091 0.04035 39.9% Y 0.04659 0.05149 0.05025 0.04842 0.05012 3.9% Zr 1.05594 1.09315 1.12866 1.10967 1.11251 2.5% Mo 0.02193 0.01663 0.01306 0.01065 0.00772 39.3% Ba 0.33311 0.28264 0.28285 0.27862 0.29248 7.6% La 0.04555 0.04562 0.04570 0.04395 0.04313 2.6%
Mo 0.19273 0.20786 0.22774 0.20275 0.22356 6.9% Ba 0.53210 0.53897 0.53534 0.53967 0.53050 0.8% La 0.56455 0.56556 0.53501 0.56600 0.53556 3.0% Ce 0.71119 0.71083 0.69686 0.71464 0.71127 1.0% 93Cav-float Rb 0.09823 0.05371 0.06815 0.04091 0.04035 39.9% Y 0.04659 0.05149 0.05025 0.04842 0.05012 3.9% Zr 1.05594 1.09315 1.12866 1.10967 1.11251 2.5% Mo 0.02193 0.01663 0.01306 0.01065 0.00772 39.3% Ba 0.33311 0.28264 0.28285 0.27862 0.29248 7.6% La 0.04555 0.04562 0.04570 0.04395 0.04313 2.6%
Ba 0.53210 0.53897 0.53534 0.53967 0.53050 0.8% La 0.56455 0.56556 0.53501 0.56600 0.53556 3.0% Ce 0.71119 0.71083 0.69686 0.71464 0.71127 1.0% 93Cav-float Rb 0.09823 0.05371 0.06815 0.04091 0.04035 39.9% Y 0.04659 0.05149 0.05025 0.04842 0.05012 3.9% Zr 1.05594 1.09315 1.12866 1.10967 1.11251 2.5% Mo 0.02193 0.01663 0.01306 0.01065 0.00772 39.3% Ba 0.33311 0.28264 0.28285 0.27862 0.29248 7.6% La 0.04555 0.04562 0.04570 0.04395 0.04313 2.6%
La 0.56455 0.56556 0.53501 0.56600 0.53556 3.0% Ce 0.71119 0.71083 0.69686 0.71464 0.71127 1.0% 93Cav-float Rb 0.09823 0.05371 0.06815 0.04091 0.04035 39.9% Y 0.04659 0.05149 0.05025 0.04842 0.05012 3.9% Zr 1.05594 1.09315 1.12866 1.10967 1.11251 2.5% Mo 0.02193 0.01663 0.01306 0.01065 0.00772 39.3% Ba 0.33311 0.28264 0.28285 0.27862 0.29248 7.6% La 0.04555 0.04562 0.04570 0.04395 0.04313 2.6%
Ce 0.71119 0.71083 0.69686 0.71464 0.71127 1.0% 93Cav-float Rb 0.09823 0.05371 0.06815 0.04091 0.04035 39.9% Y 0.04659 0.05149 0.05025 0.04842 0.05012 3.9% Zr 1.05594 1.09315 1.12866 1.10967 1.11251 2.5% Mo 0.02193 0.01663 0.01306 0.01065 0.00772 39.3% Ba 0.33311 0.28264 0.28285 0.27862 0.29248 7.6% La 0.04555 0.04562 0.04570 0.04395 0.04313 2.6%
93Cav-float Rb 0.09823 0.05371 0.06815 0.04091 0.04035 39.9% Y 0.04659 0.05149 0.05025 0.04842 0.05012 3.9% Zr 1.05594 1.09315 1.12866 1.10967 1.11251 2.5% Mo 0.02193 0.01663 0.01306 0.01065 0.00772 39.3% Ba 0.33311 0.28264 0.28285 0.27862 0.29248 7.6% La 0.04555 0.04562 0.04570 0.04395 0.04313 2.6%
Rb 0.09823 0.05371 0.06815 0.04091 0.04035 39.9% Y 0.04659 0.05149 0.05025 0.04842 0.05012 3.9% Zr 1.05594 1.09315 1.12866 1.10967 1.11251 2.5% Mo 0.02193 0.01663 0.01306 0.01065 0.00772 39.3% Ba 0.333311 0.28264 0.28285 0.27862 0.29248 7.6% La 0.04555 0.04562 0.04570 0.04395 0.04313 2.6%
Rb 0.09823 0.05371 0.06815 0.04091 0.04035 39.9% Y 0.04659 0.05149 0.05025 0.04842 0.05012 3.9% Zr 1.05594 1.09315 1.12866 1.10967 1.11251 2.5% Mo 0.02193 0.01663 0.01306 0.01065 0.00772 39.3% Ba 0.333311 0.28264 0.28285 0.27862 0.29248 7.6% La 0.04555 0.04562 0.04570 0.04395 0.04313 2.6%
Y 0.04659 0.05149 0.05025 0.04842 0.05012 3.9% Zr 1.05594 1.09315 1.12866 1.10967 1.11251 2.5% Mo 0.02193 0.01663 0.01306 0.01065 0.00772 39.3% Ba 0.33311 0.28264 0.28285 0.27862 0.29248 7.6% La 0.04555 0.04562 0.04570 0.04395 0.04313 2.6%
Zr 1.05594 1.09315 1.12866 1.10967 1.11251 2.5% Mo 0.02193 0.01663 0.01306 0.01065 0.00772 39.3% Ba 0.33311 0.28264 0.28285 0.27862 0.29248 7.6% La 0.04555 0.04562 0.04570 0.04395 0.04313 2.6%
Mo 0.02193 0.01663 0.01306 0.01065 0.00772 39.3% Ba 0.33311 0.28264 0.28285 0.27862 0.29248 7.6% La 0.04555 0.04562 0.04570 0.04395 0.04313 2.6%
Ba 0.33311 0.28264 0.28285 0.27862 0.29248 7.6% La 0.04555 0.04562 0.04570 0.04395 0.04313 2.6%
La 0.04555 0.04562 0.04570 0.04395 0.04313 2.6%
89GrandAm-float
Rb 0.03655 0.04952 0.04259 0.03711 0.02751 21.0%
Y 0.03194 0.03240 0.03078 0.03254 0.03241 2.3%
Zr 0.71778 0.74371 0.71745 0.72959 0.74367 1.8%
Mo 0.01086 0.00902 0.00793 0.00540 0.00641 27.1%
VIOLOGO VIOUVOM VIOUVOM VIOUVOM VIOUVOM 2/1/U

Table 3, continued. Sr-normalized Peak Heights for analyses.

	86LabGTS-float					
Rb	1.05561	1.10841	1.10322	1.12363	1.09350	2.3%
Y	0.09565	0.09627	0.10173	0.09955	0.09953	2.6%
Zr	0.84067	0.88279	0.89762	0.88877	0.93635	3.9%
Mo	0.02191	0.01179	0.01420	0.01268	0.00989	32.9%
Ba	2.11178	2.24842	2.25134	2.29036	2.32543	3.6%
La	0.14090	0.15426	0.14814	0.15353	0.15541	4.0%
Ce	0.37037	0.38477	0.38390	0.39192	0.38768	2 .1%
	95Cont-float					
Rb	0.05462	0.04955	0.04074	0.03208	0.06919	28.6%
Y	0.08696	0.09048	0.08824	0.09028	0.08948	1.7%
Zr	3.21206	3.22940	3.20355	3.30166	3.23587	1.2%
Mo	0.01188	0.01849	0.00966	0.00923	0.00636	41.0%
Ba	0.29792	0.26795	0.26933	0.26128	0.25994	5.7%
La	0.04409	0.04412	0.04299	0.04305	0.04433	1.5%
Ce	0.12216	0.11532	0.11266	0.11157	0.12207	4.4%
	90Beretta-float					
Rb	0.06387	0.06960	0.04558	0.05516	0.04502	19.5%
Y	0.01747	0.01806	0.01689	0.01821	0.01819	3.2%
Zr	0.20864	0.20503	0.20676	0.20578	0.20844	0.8%
Mo	0.01121	0.00905	0.00776	0.00872	0.00987	13.9%
Ba	0.27710	0.25154	0.24776	0.26512	0.29144	6.8%
La	0.05971	0.06048	0.06015	0.06200	0.06235	1.9%
Ce	0.15400	0.15288	0.15183	0.15339	0.15033	0.9%
	90Accord-float					
Rb	0.06842	0.05471	0.04956	0.05532	0.05144	13.2%
Y	0.02148	0.02206	0.02266	0.02249	0.02202	2.1%
Zr	0.36716	0.37068	0.38913	0.37247	0.37130	2.3%
Мо	0.01036	0.00618	0.00964	0.00590	0.00499	<i>32.6%</i>
Ba	0.26823	0.25225	0.25665	0.25212	0.23285	5.1%
La	0.03309	0.03368	0.03455	0.03476	0.03228	3.1%
Се	0.09057	0.08784	0.08685	0.09900	0.08458	6.2%
Phase III					_	
	NIST 612	npie and peak/	Sr for each rep	piicate (n=5)	R	SD %
Y	0.46124	0.45984	0.46893	0.45687	0.45574	1.1%
Zr	0.23138	0.23508	0.23328	0.22704	0.23154	1.3%
Ba	0.52378	0.53865	0.52422	0.52213	0.54552	2.0%
La	0.60107	0.59872	0.57807	0.58658	0.59632	1.6%
Ce	0.73008	0.72518	0.70878	0.70323	0.71892	1.6%
	85Brougham					
Y	0.02814	0.02760	0.02822	0.02844	0.02752	1.4%
Zr	0.99588	0.97983	1.00389	1.01014	1.00165	1.2%
Ba	0.26023	0.20711	0.20885	0.20186	0.20446	11.4%
La	0.03097	0.02822	0.02827	0.02662	0.02633	6.6%
Ce	0.07629	0.06678	0.06047	0.05818	0.05836	12.0%
	0.07027	0.00070	0.00017	0.00010	0.0000	. 2.070

 Table 3, continued. Sr-normalized Peak Heights for analyses.

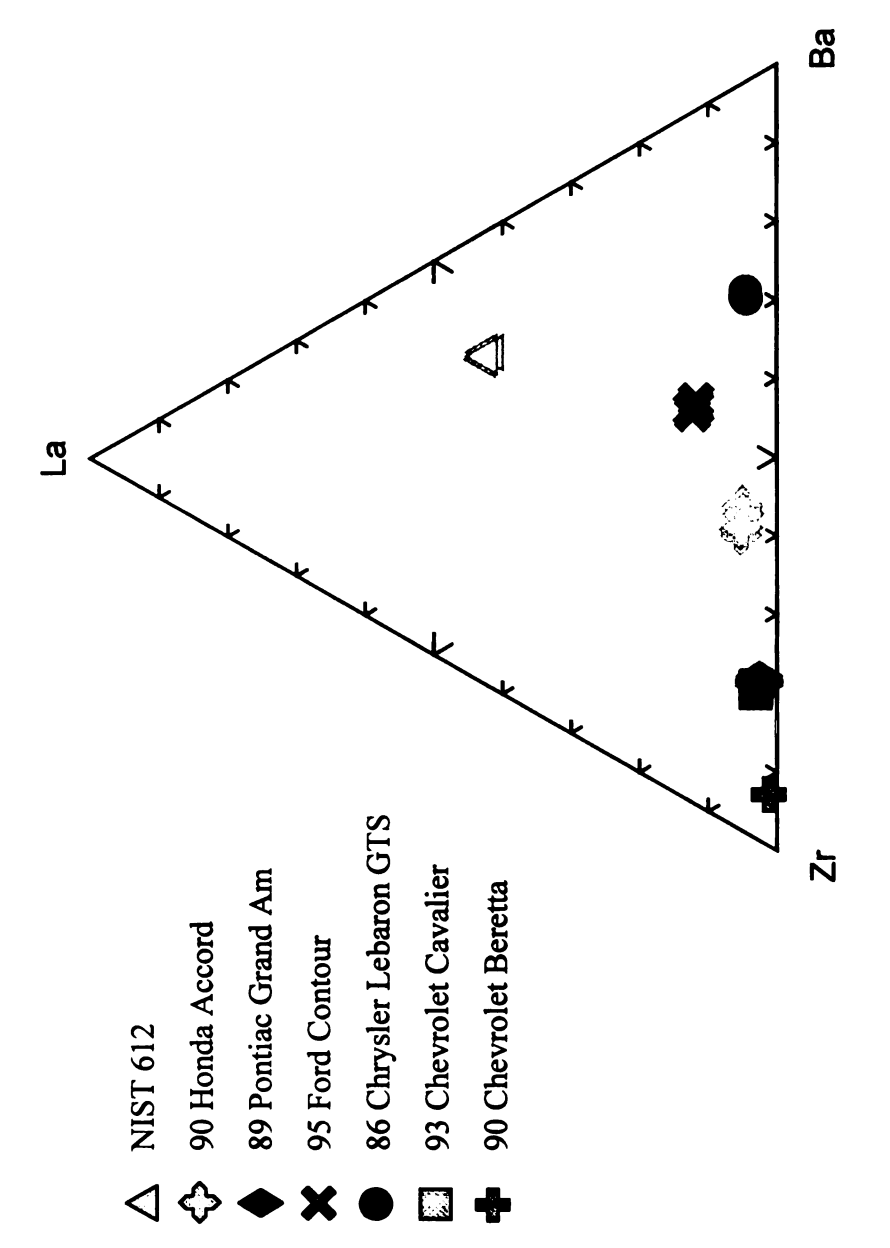
	85Brougham-float					
Y	0.02916	0.02924	0.02952	0.02813	0.02892	1.8%
Zr	1.10373	1.10724	1.11818	1.06757	1.10663	1.8%
Ba	0.20893	0.28705	0.20611	0.20403	0.20163	16.6%
La	0.02827	0.02661	0.02682	0.02661	0.02594	<i>3.2%</i>
Ce	0.05917	0.06212	0.05378	0.05629	0.05665	<i>5.5%</i>
	89Sundance					
Y	0.06414	0.06501	0.06791	0.06615	0.06601	2.1%
Zr	0.76770	0.74801	0.78686	0.77094	0.76171	1.8%
Ba	0.31991	0.28210	0.28137	0.27431	0.27080	6.9%
La	0.07346	0.07598	0.07169	0.07096	0.07065	3.0%
Ce	0.15916	0.15013	0.14397	0.14299	0.14642	4.4%
	89Sundance-float					
Y	0.06452	0.06850	0.06611	0.06884	0.06785	2.7%
Zr	0.73644	0.78412	0.78224	0.80346	0.76869	3.2%
Ba	0.26680	0.26928	0.26651	0.27526	0.26991	1.3%
La	0.06634	0.20728	0.07311	0.07276	0.07270	4.0%
Ce	0.14583	0.14227	0.14850	0.14271	0.14755	1.9%
CC	0.14383	0.17227	0.14850	0.14271	0.14733	1.770
	94Metro					
Y	0.03502	0.03594	0.03692	0.03575	0.03496	2.2%
Zr	0.68983	0.70041	0.68880	0.70881	0.71257	1.5%
Ba	0.17839	0.17343	0.17083	0.17790	0.17547	1.8%
La	0.04415	0.04447	0.04469	0.04524	0.04389	1.2%
Ce	0.14716	0.14215	0.14227	0.14209	0.14124	1.7%
	0.004					
	94Metro-float					
Y	0.03408	0.03534	0.03599	0.03674	0.03381	3.5%
Zr	0.65288	0.66554	0.69552	0.66802	0.65499	2.6%
Ba	0.17803	0.16908	0.17669	0.17068	0.17579	2.3%
La	0.04502	0.04389	0.04545	0.04132	0.04302	<i>3.8%</i>
Се	0.14155	0.13904	0.13965	0.13770	0.14115	1.1%
	90Sunbird					
Y	0.02507	0.02589	0.02626	0.02632	0.02638	2.1%
Zr	0.40343	0.40193	0.40777	0.41634	0.41796	1.8%
Ba	0.23556	0.21910	0.22804	0.23115	0.22605	2.7%
La	0.06785	0.03857	0.03856	0.03848	0.03799	29.7%
Ce	0.09302	0.08603	0.08829	0.08699	0.08635	3.2%
CC	0.07502	0.00003	0.00027	0.00077	0.00055	3.270
	90Sunbird-float					
Y	0.02405	0.02677	0.02467	0.02660	0.02570	4.6%
Zr	0.40728	0.41518	0.41545	0.42691	0.41712	1.7%
Ba	0.23638	0.22132	0.22122	0.22310	0.21371	3.7%
La	0.03588	0.03876	0.03925	0.03926	0.03680	4.1%
Ce	0.08417	0.08461	0.08625	0.08406	0.08392	1.1%

importance of replicate values is apparent, as when the first of the five replicates is removed, the precision RSD decreases to 0.7%. Graphical plots of the data allow for quick recognition of such uncommon imprecise analyses by comparing relative proportions of each element in a sample.

Element proportions were compared using ternary diagrams plotted with IgPet for Windows®, a geological plotting software package (Terra Softa Inc., New Jersey, U.S.A). In each diagram, integrated peak heights are plotted for three elements. The location of a sample in the triangle represents the relative proportion of each of the three elements with respect to the other two. Therefore a sample plotting in the center of the triangle, equidistant from each of the three apexes (X, Y, and Z), would have a relative composition of approximately 33.3% X, 33.3% Y and 33.3% Z.

Precision and Discrimination

The results from the first set of analyses (Phase I) on six unknown fragments and NIST 612 are presented in Figure 1, showing relative peak heights of Zr, La and Ba for each sample. Each symbol represents one analysis for the non-float side of a given fragment. Each sample was ablated five times to determine precision. Precision for this set of analyses is good (except for Rb and Mo in several samples, as described above). Aside from low RSD values (Table 3), the precision can be evaluated graphically by the relatively tight grouping of replicate analyses in Figure 1. Notice that the only two samples that are not clearly differentiated by ratios of these three elements are 89GrandAm and 93Cav. Both samples have relatively low counts of La, plotting near the Zr-Ba axis with similar proportions of those two elements. In this diagram, the samples



Phase I. Symbols represent five replicate analyses for each sample on the non-float side Figure 1. Plot of all analyses for the set of six unknown fragments and NIST 612 from of fragments. Note that only two samples, 89GrandAm and 93Cav, are not clearly differentiated using these three elements (Zr-La-Ba).

overlap within the range of the precision of the samples and cannot be clearly differentiated. However, when La is replaced with a more abundant element, Sr, the two samples separate (Figure 2). Using only these three elements (Zr-Sr-Ba), all six unknown samples can be clearly differentiated.

Although the precision decreased slightly for several elements in select samples, the results from analyses of the float side of the same six unknown fragments in Phase II were very similar to those from Phase I. The RSD values for replicate measurements remained less than 10% for all elements (Table 3). Using the same Zr-Sr-Ba plot as used for the non-float analyses (Figure 2), all six samples are still clearly distinguished from one another, even with slightly lower precision (Figure 3). In this diagram, for example, one of the five 93Cav (open squares) analyses plots slightly closer toward the Sr-Ba axis than the others, which is reflected in the slightly higher RSD value (7.6% vs.5.1% in Phase I, Table 3). However, the significant overlap of this data point with other replicate measurements for the sample forms a tight cluster that is plainly dissimilar from other samples.

Analyses from the non-float (Phase I) and float (Phase II) sides, which were acquired eight months apart, are shown together in Figure 4. Note that although there is slight drift for some samples (e.g. 95Cont), the range for all samples remains quite narrow. Analyses for individual samples still form distinct clusters. Table 4 gives precision RSD values for elements in each sample using analyses from both Phase I and Phase II. RSD values remain below 10%, with the exception of a value of 10.1% RSD for Ce in one sample (90Beretta). Remarkably, the molten tin in the float process does not

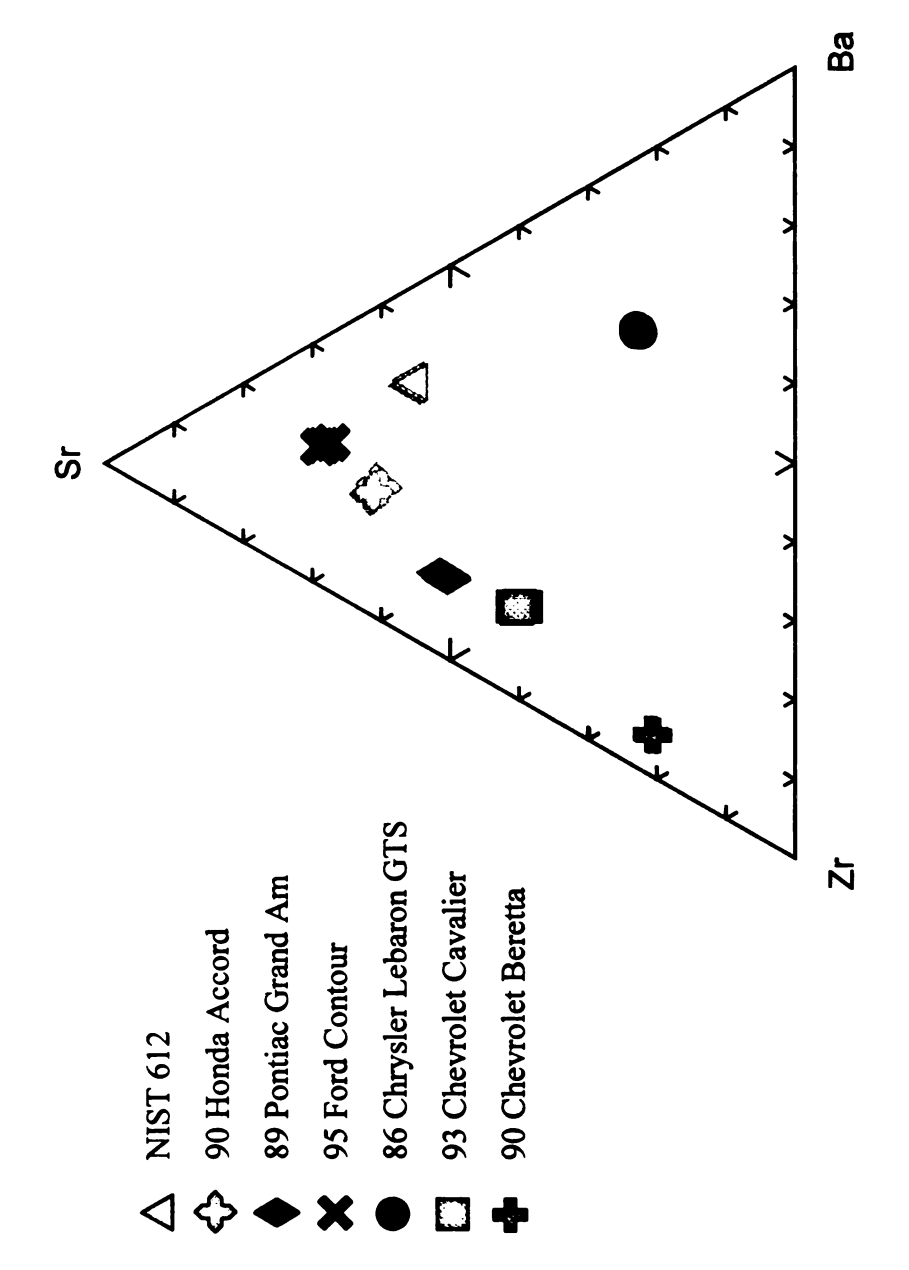
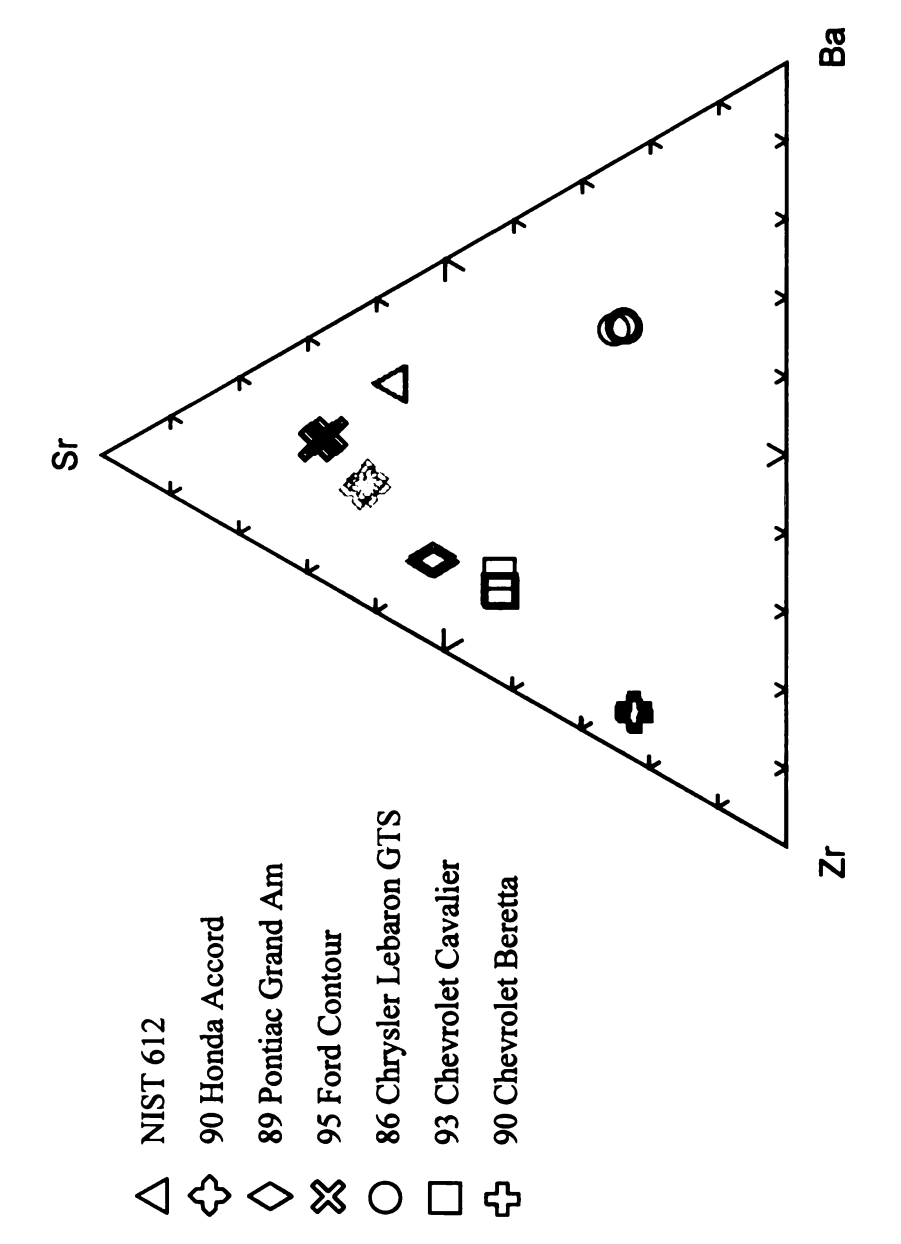


Figure 2. Plot of all analyses for the set of six unknown fragments and NIST 612 from Figure 1. Notice that all samples, including 89GrandAm and 93Cav from Figure 1 are Phase I, replacing La in Figure 1 with Sr at the top apex. Symbols are the same as clearly separated.



Phase II. Symbols represent five replicate analyses for each sample on the float side of Figure 3. Plot of all analyses for the set of six unknown fragments and NIST 612 from fragments.

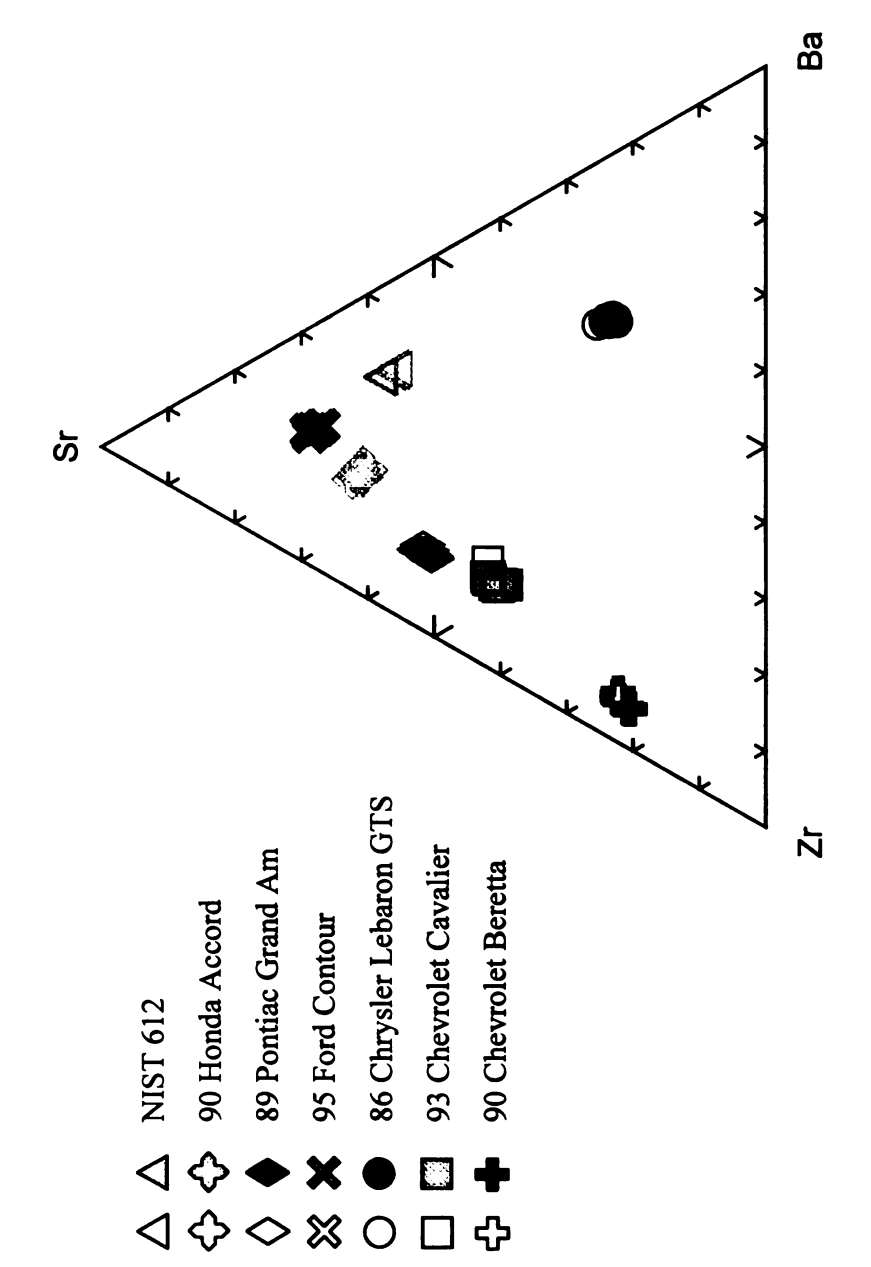


Figure 4. Plot of all analyses for the set of six unknown fragments and NIST 612 from sample on the non-float side of fragments (Phase I) while open symbols represent five both Phase I and Phase II. Closed symbols represent five replicate analyses for each replicate analyses on the float side of fragments (Phase II).

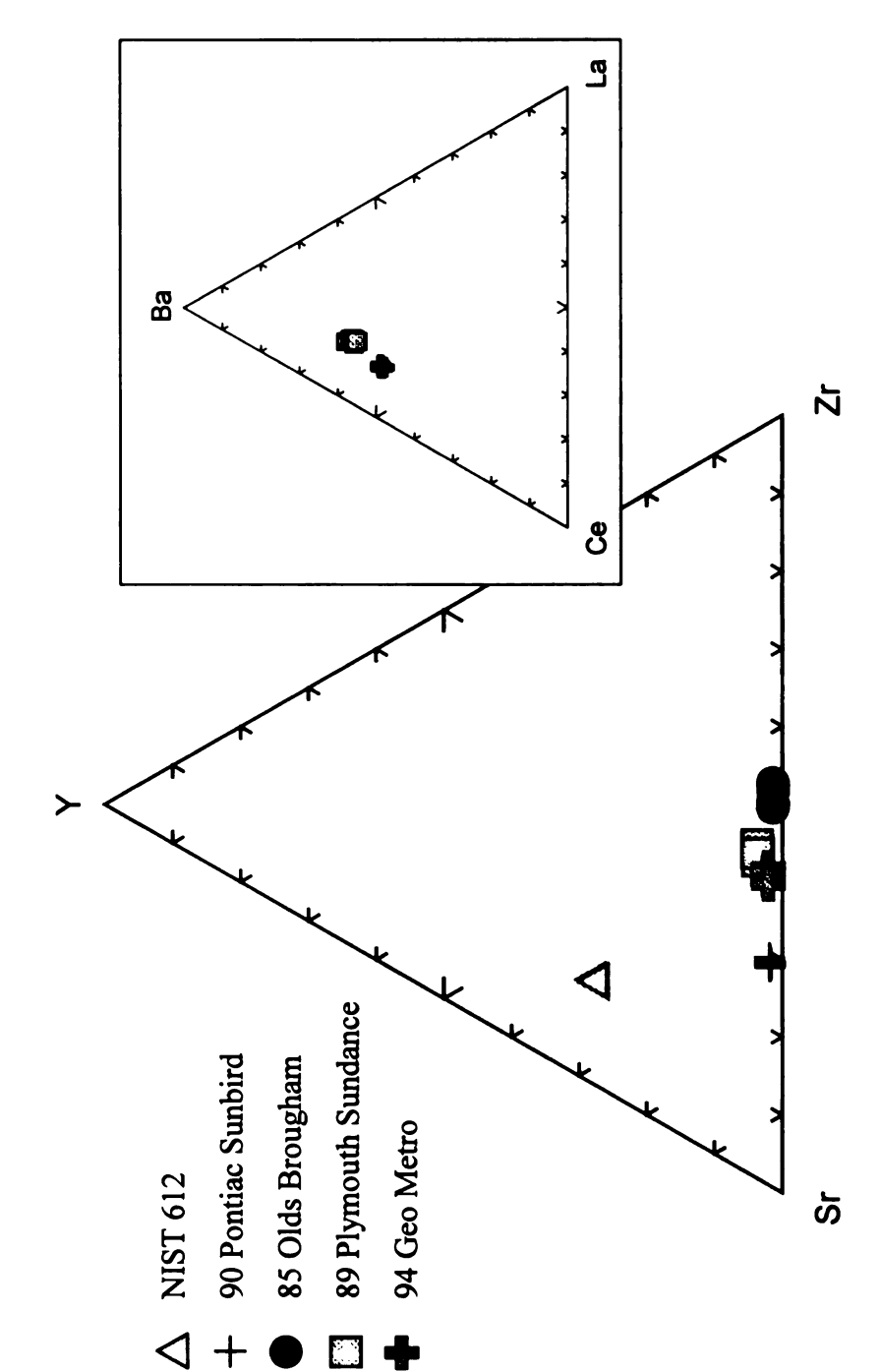
	NIST 612	93Cav	89GrandAm	86LabGTS	95Cont	90Beretta	90Accord
	n=10	n=10	n=10	n=10	n=10	n=10	n=10
Rb	6.3%	57.6%	30.1%	2.6%	27.7%	16.4%	19.4%
Y	2.2%	3.6%	3.6%	7.9%	1.9%	3.9%	3.0%
Zr	3.0%	5.3%	3.3%	%5'5	%8'5	78%	2.0%
Мо	8.6%	46.4%	40.2%	38.8%	35.1%	21.2%	38.3%
Ba	5.3%	6.1%	2.9%	%0'\$	4.9%	%6'\$	%0.9
La	4.3%	3.0%	2.2%	4.4%	3.2%	3.1%	2.8%
ප	8.0%	3.6%	4.6%	%8'9	4.9%	10.1%	6.7%

in Phase I and II. Each RSD value includes five replicate analyses on the non-float Table 4. Precision RSD values for non-float and float side analyses for all samples side and five analyses on the float side of each fragment. RSD values are given for peak heights normalized to Sr.

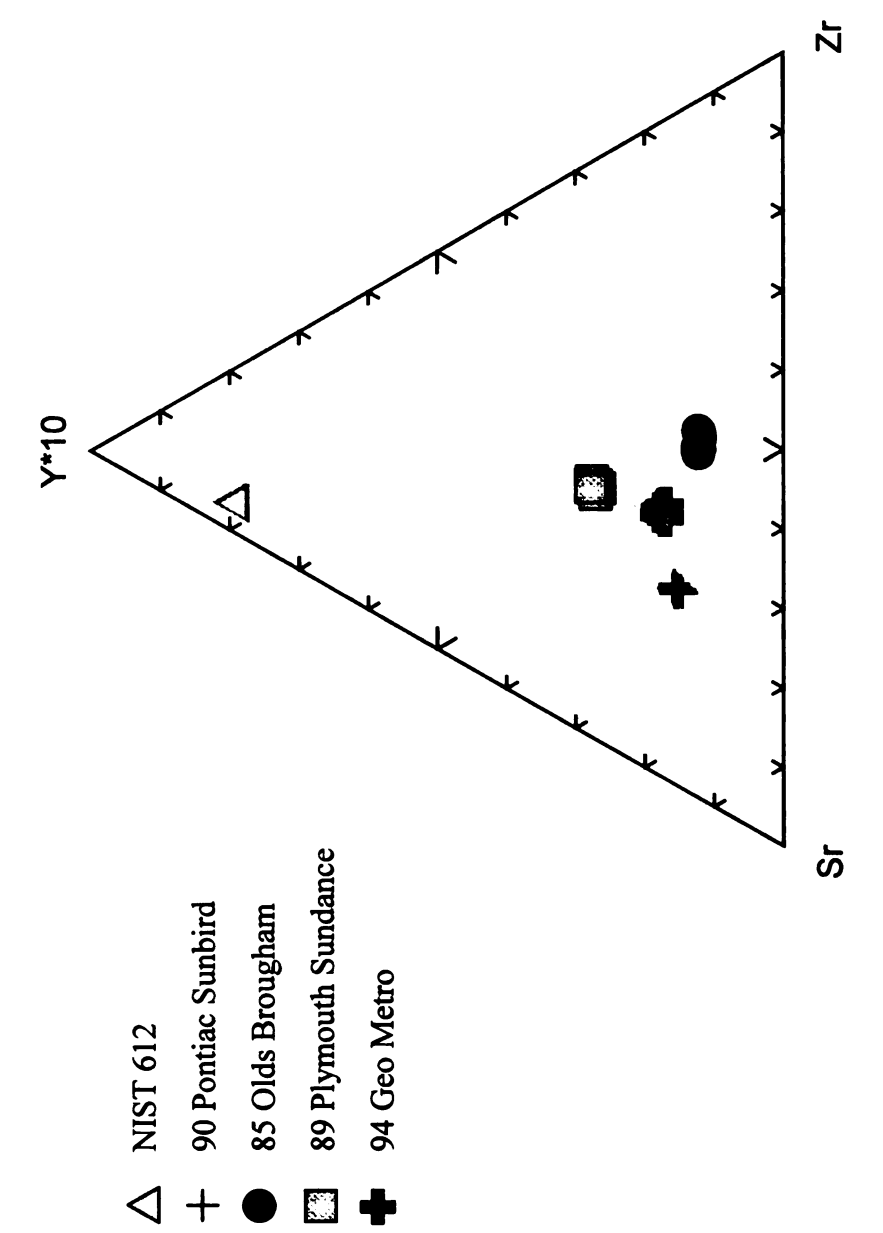
appear to affect the measured trace element ratios of the glass by imparting additional elements to the float side, as is observed with Sn.

Results for the analyses of the second subset of samples in Phase III of the experiment are given in Figure 5. Data points include five analyses conducted on the float side and five analyses of the non-float side of each sample for a total of 10 analyses. Note that a different set of elements is used in this comparison (Sr-Y-Zr) than in Figures 2-4 (Zr-Sr-Ba), as they provided the better discrimination between all four samples. The four samples plot in distinct groups, with slight overlap between two samples (89Sundance and 94Metro). Again, using another group of elements (e.g. Ce-Ba-La, inset Figure 5), these samples can be clearly separated. However, samples with roughly similar peak heights of one element can also be differentiated by modifying the relative value of the component, as suggested by Watling et al. (1997). Figure 6 demonstrates this effect by multiplying Y by a factor of ten. All peak values are multiplied by the same value, resulting in separation of different groups while maintaining the precision of replicate measurements.

Figure 7 shows the entire set of ten samples. Note that only two samples, 90Accord and 90Sunbird, cannot be excluded as having come from the same source. Using the six elements in the abbreviated menu (88Sr, 89Y, 90Zr, 138Ba, 139La, and 140Ce) and four additional isotopes (46Ti, 55Mn, 177Hf, and 208Pb), these two samples could not be distinguished from one another graphically. However, the samples were known to be different based on thickness measurements (90Accord, 2.04 mm; and 90Sunbird, 2.24 mm). The samples were also discriminated using simple t-tests comparing population means of measured elemental ratios in each sample at the 95% confidence level (P<0.05).



Note that the fragments that are not clearly discriminated in the plot (Sr-Y-Zr) can be five replicates on the non-float side and five replicates on the float side of fragments. NIST 612 from Phase III. Symbols represent ten replicate analyses for each sample, Figure 5. Plot of all analyses for the set of additional four unknown fragments and differentiated using an additional three elements (Ce-Ba-La, inset).



NIST 612 from Phase III showing the effect of multiplying one component (Y) by a Figure 6. Plot of all analyses for the set of additional four unknown fragments and factor of ten. Symbols are the same as Figure 5.

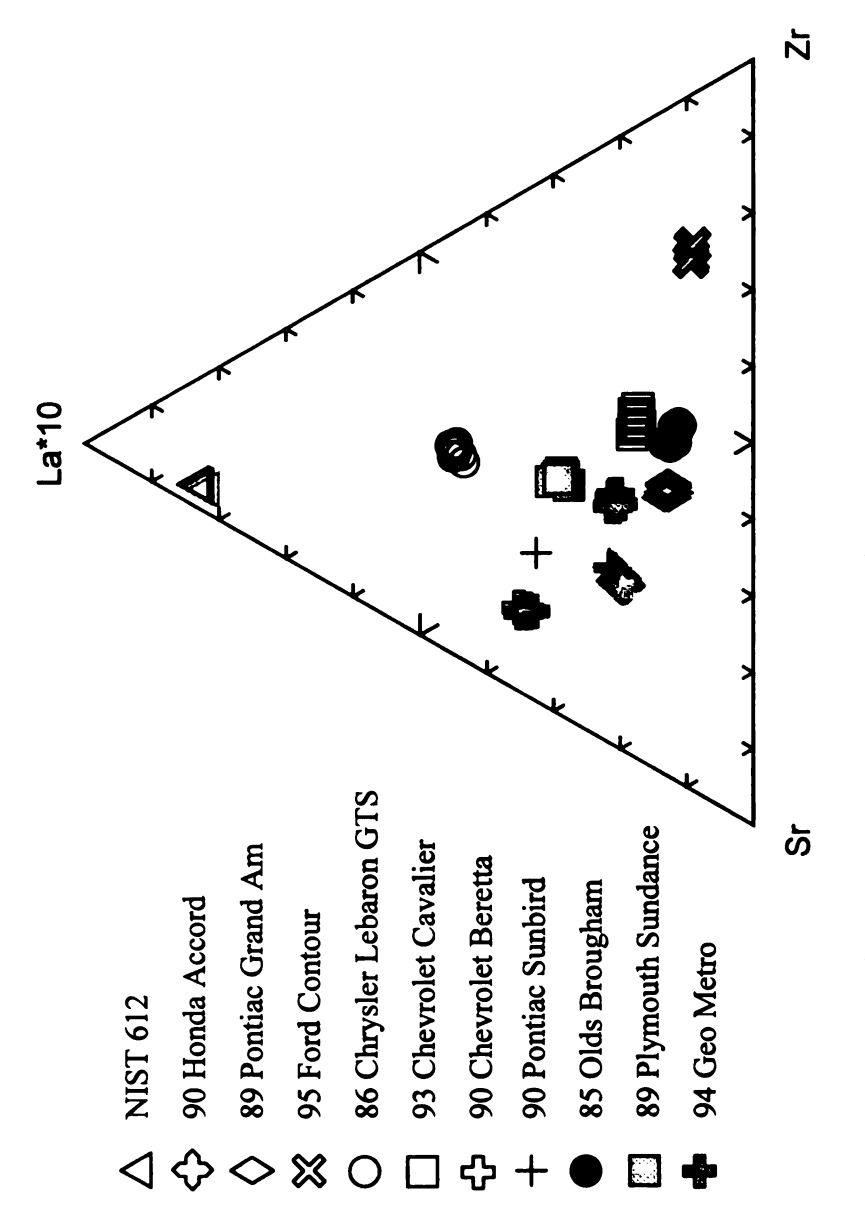
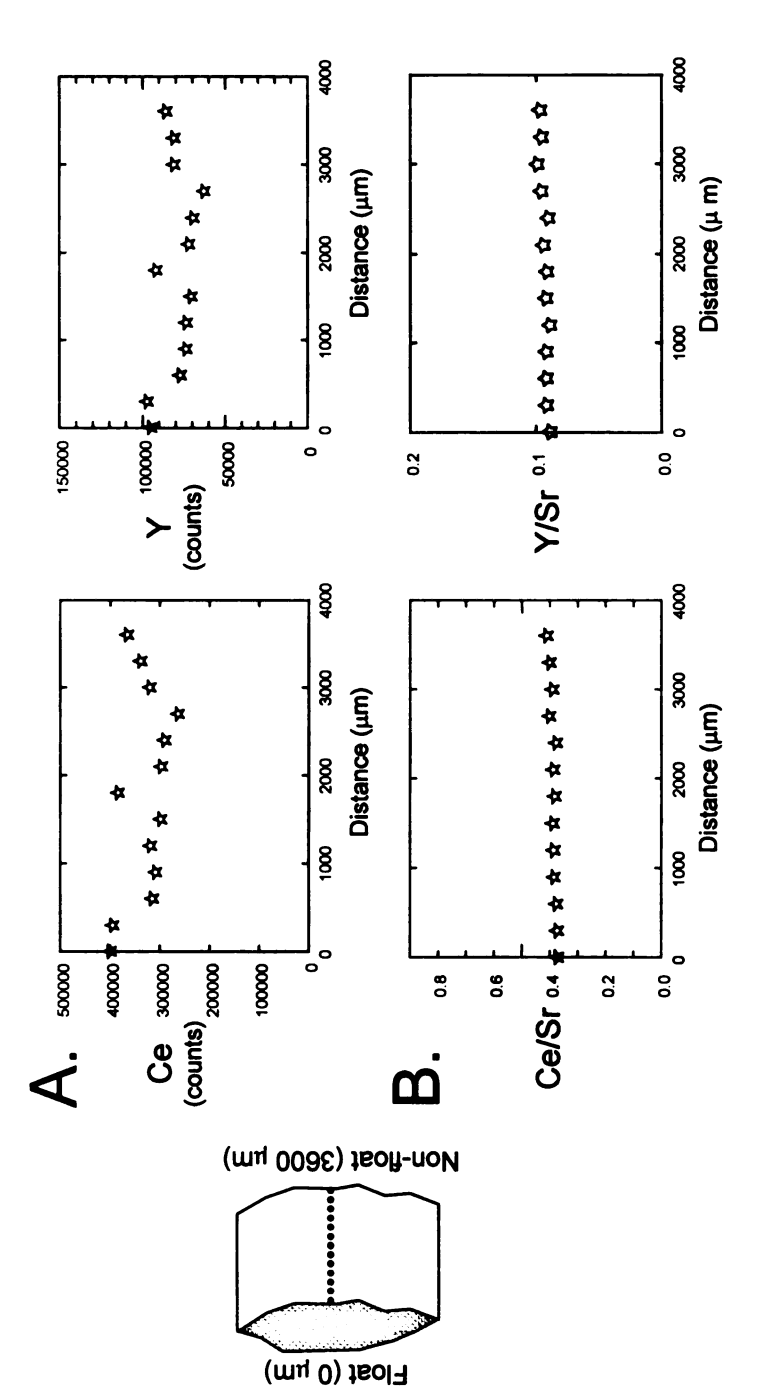


Figure 7. Plot of all analyses for the entire set of ten unknown fragments and NIST 612 from Phase I, II, and III. Symbols represent ten replicate analyses for each sample, five replicates on the non-float side and five replicates on the the float side of fragments. See text for discussion of samples 90Accord and 90Sunbird, which cannot be graphically discriminated using any combination of elements.

There are two feasible explanations for the similarity of these two samples. First, the samples may have come from completely different sources and by chance have a trace element composition that cannot readily be differentiated using the graphical method. Alternatively, the glasses may have come from the same manufacturer, having been produced at different times on the same float line (explaining the different thicknesses but similar trace element compositions). However, the vehicles from which these samples originated were manufactured in Sayama, Japan (90Accord) and Lordstown, OH, USA (90Sunbird). Unless the glass from the 1990 Accord was installed after-market, it appears unlikely that the second option is the case. The similarity of these two samples merits further investigation, as the first option is the preferred explanation.

Precision and Sample Homogeneity

In each of the second and third phases of the experiment, a cross-sectional traverse of one fragment was conducted to ensure reproducibility of measurements through the thickness of the sample. In Phase II, sample 86LabGTS was ablated 13 times in a line perpendicular to its parallel sides, with ablation spots 300 µm apart. Figure 8 shows a schematic diagram of the fragment and distance between ablation points plotted against raw peak heights (in counts) for Ce and Y, as well as ratios for Ce/Sr and Y/Sr. There is variability from analysis to analysis in the raw peak heights for each element (Figure 8a), but normalization to one element (Sr) has a smoothing effect on the data (Figure 8b). Although many factors influence elemental signals in an analysis (laser power, sample coupling, etc.), the ratio of counts between two elements should remain



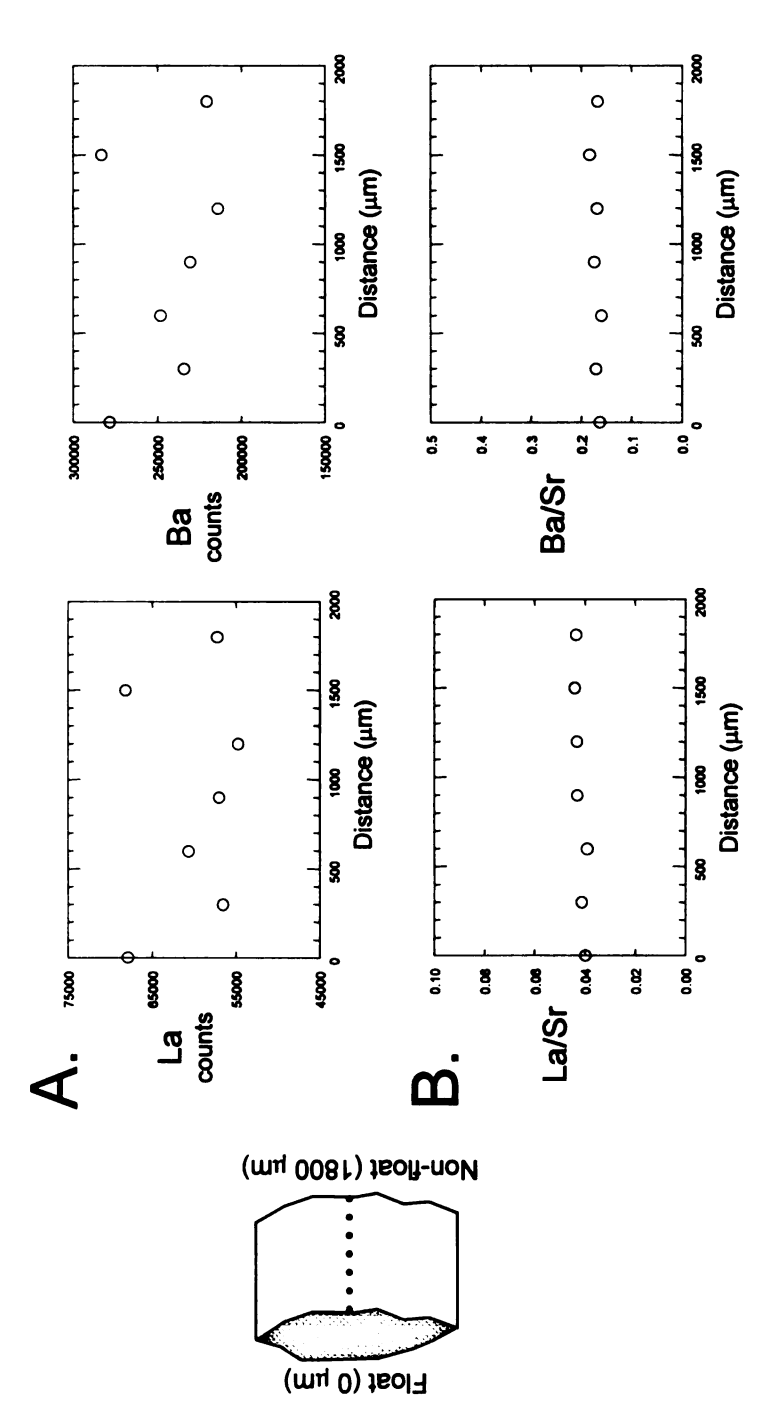
of distance versus peak height (counts) for Ce and Y along the cross-section. B. Plot of Phase II. Analyses were spaced 300 µm apart for a total of 13 ablation points. A. Plot Figure 8. Schematic diagrams of cross-sectional traverses of sample 86LabGTS from distance versus peaks heights for Ce and Y normalized to Sr. Note the relative flat profiles using normalized values.

approximately constant, assuming minimal fractionation effects (Trejos and Almirall, 2004). This effect is observed in the relatively flat profiles in Figure 8b.

Similar profiles are seen for a cross section of sample 94Metro (Figure 9), which was analyzed in Phase III, seven months after the cross-section for sample 86LabGTS. Again, ablation spots were spaced 300 µm apart. The inconsistency of analyses in terms of raw peak counts for La and Ba (Figure 9a) is greatly diminished when analyses are normalized to Sr (Figure 9b). Given the relatively flat profiles in Figures 8b and 9b, replicate measurements of trace element ratios through sample transects are considered both precise and homogeneous. The precision RSD values (88Srnormalized) for all elements within an entire transect are ~5% or less (Table 5). In addition to the compositional homogeneity demonstrated between the float and non-float sides of fragments in the previous section, these results show that the technique is precise even in cases where no parallel sides are present, as is often true of casework samples, where only irregularly shaped questioned fragments are found.

APPLICATION OF THE METHOD: CASEWORK EXAMPLES

Since completion of the experiments and evaluation of the results, the technique has been applied to casework for the Michigan State Police Forensic Laboratory in Lansing, MI, U.S.A. In cases where fragments cannot be discriminated on the basis of physical properties, such as refractive index, or major element composition as determined by SEM-EDS, trace element ratios are determined by LA-ICP-MS. The following case examples demonstrate the discriminatory and associative power of the method. In cases where an exclusion is made, the analytical scheme is improved by eliminating Type II



Plot of distance versus peaks heights for La and Ba normalized to Sr. Again, note the Phase III. Analyses were spaced 300 µm apart for a total of seven ablation points. A. Plot of distance versus peak height (counts) for La and Ba along the cross-section. B. Figure 9. Schematic diagrams of cross-sectional traverses of sample 94Metro from relative flat profiles using normalized values.

	86LabGTS	94Metro
	n=13	L=u
Y	3.4%	4.2%
Zr	8.1%	%1.5
Ba	3.7%	3.4%
La	2.2%	4.5%
ಲ	3.0%	3.2%

Table 5. Precision RSD values for analyses in two cross-sectional traverses in Phases I and II. RSD values are given for peak heights normalized to Sr.

errors. In cases where an inclusion is inferred, the association between glass fragments is greatly improved by reducing the size of the class to which they belong.

Case #1: Lansing, MI Homicide

A 26 year-old man from Lansing, Michigan was accused of shooting and killing his former wife. She was found dead on a sidewalk, several meters from her parked vehicle and just two blocks from her home. Two samples were submitted: one questioned fragment removed from the victim's scalp and multiple known fragments taken from her vehicle. The questioned fragment, three fragments of the known glass, and NIST 612 were analyzed in triplicate to demonstrate reproducibility of measurements. Figure 10 shows one of the diagrams used to conclude that the known and the questioned fragments were consistent in elemental composition and could have come from the same source. Replicate analyses for each sample plot directly on top of one another, and no combination of the six elements (⁸⁸Sr, ⁸⁹Y, ⁹⁰Zr, ¹³⁸Ba, ¹³⁹La, and ¹⁴⁰Ce) provided discrimination between the samples.

Case #2: Saginaw, MI Homicide

A 20 year-old resident of Saginaw, Michigan, was accused of breaking and entering the home of elderly man in December of 2003, killing the homeowner during the suspected robbery and then stealing the man's vehicle. Three samples were submitted for comparison: one known glass fragment obtained from the south window of the home, one questioned glass fragment found on the front porch of the home, and a second questioned fragment removed from the handle of a hammer that was suspected to have been used to

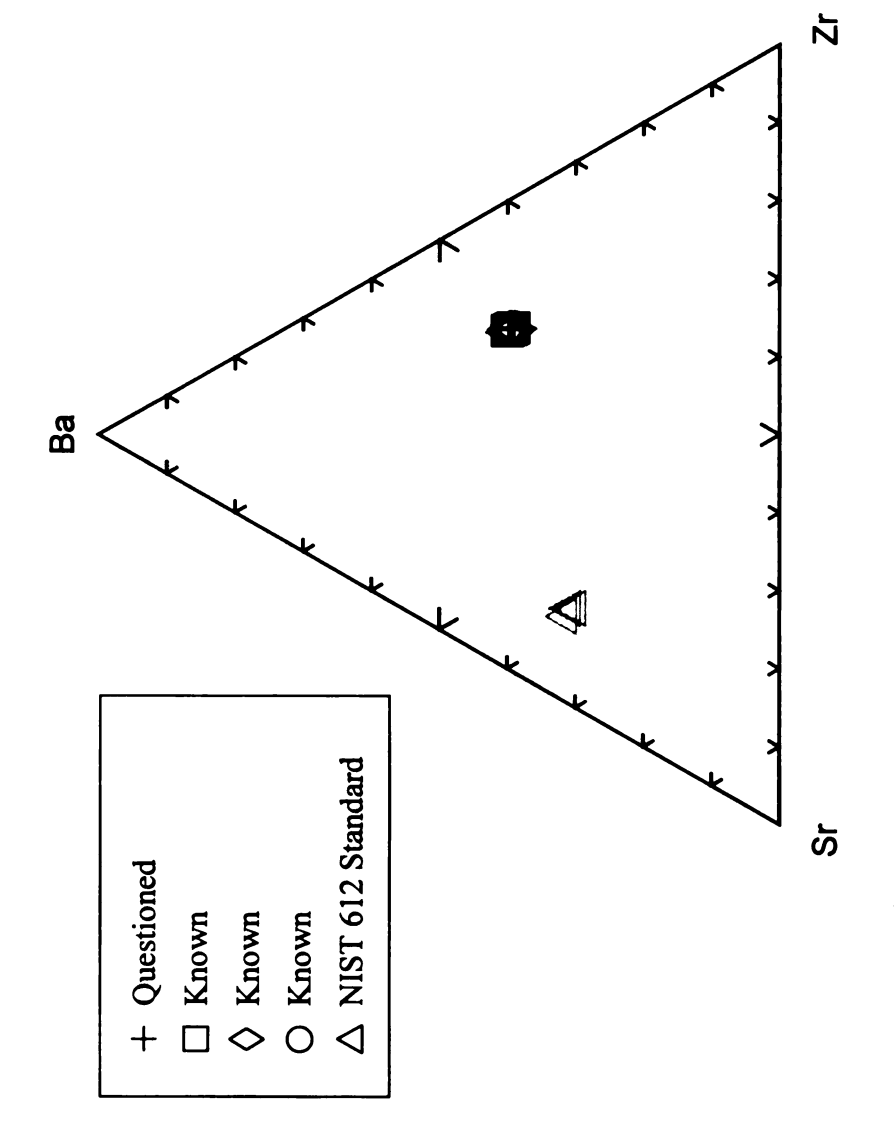


Figure 10. Plot showing one of the diagrams used to conclude that the questioned and Each sample was analyzed three times. Combinations of other elements produced the known fragments in the homicide case could have originated from the same source. same results; none of the fragments could be discriminated.

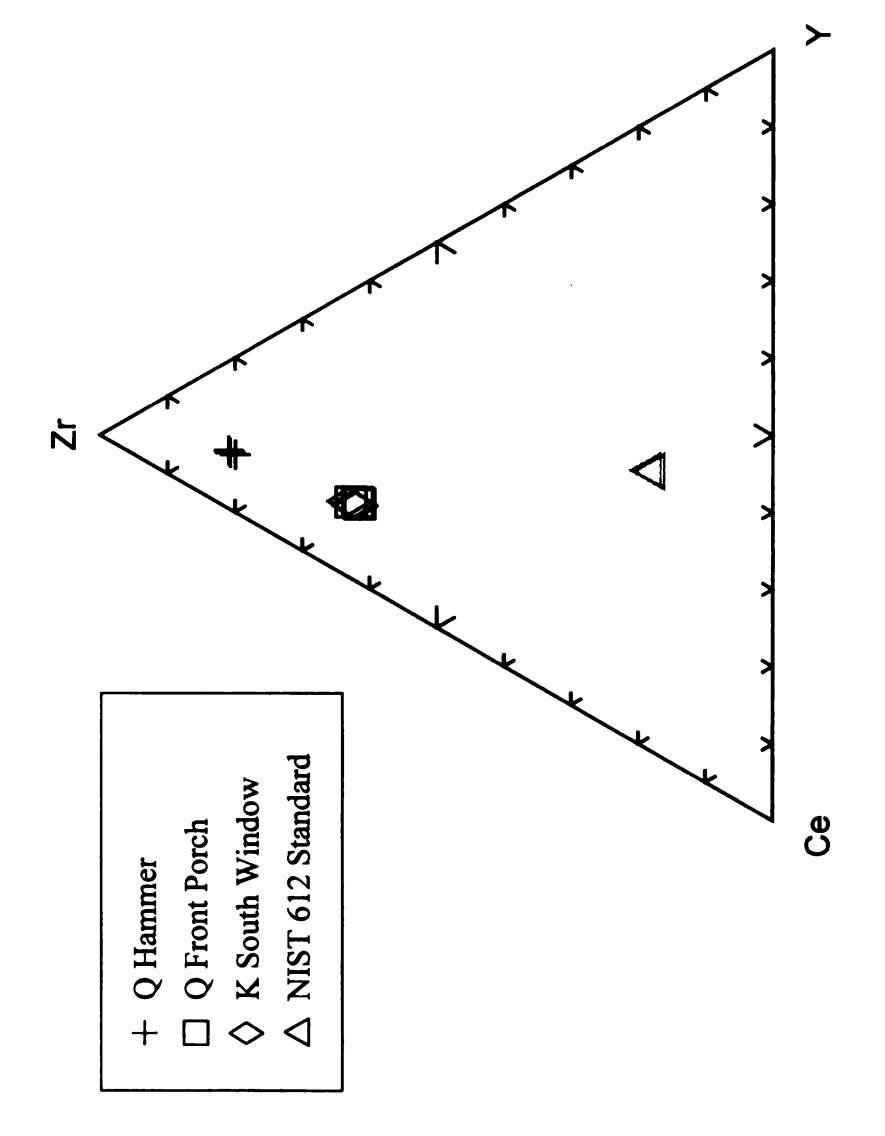
gain entry into the home through the boarded south window. Again, all three fragments and NIST 612 were ablated three times each demonstrate reproducibility, especially on the fragment from the hammer handle, which was irregularly shaped and less than 1 mm in its largest dimension. In this case, one of the questioned fragments could be distinguished from the known fragment (Q Hammer) while the other (Q Front Porch) could not (Figure 11). It was concluded that the questioned fragment from the hammer handle did not originate from the same source as the known fragment, while the fragment from the front porch could have come from that source.

Case #3: Dundee, MI Breaking and Entering

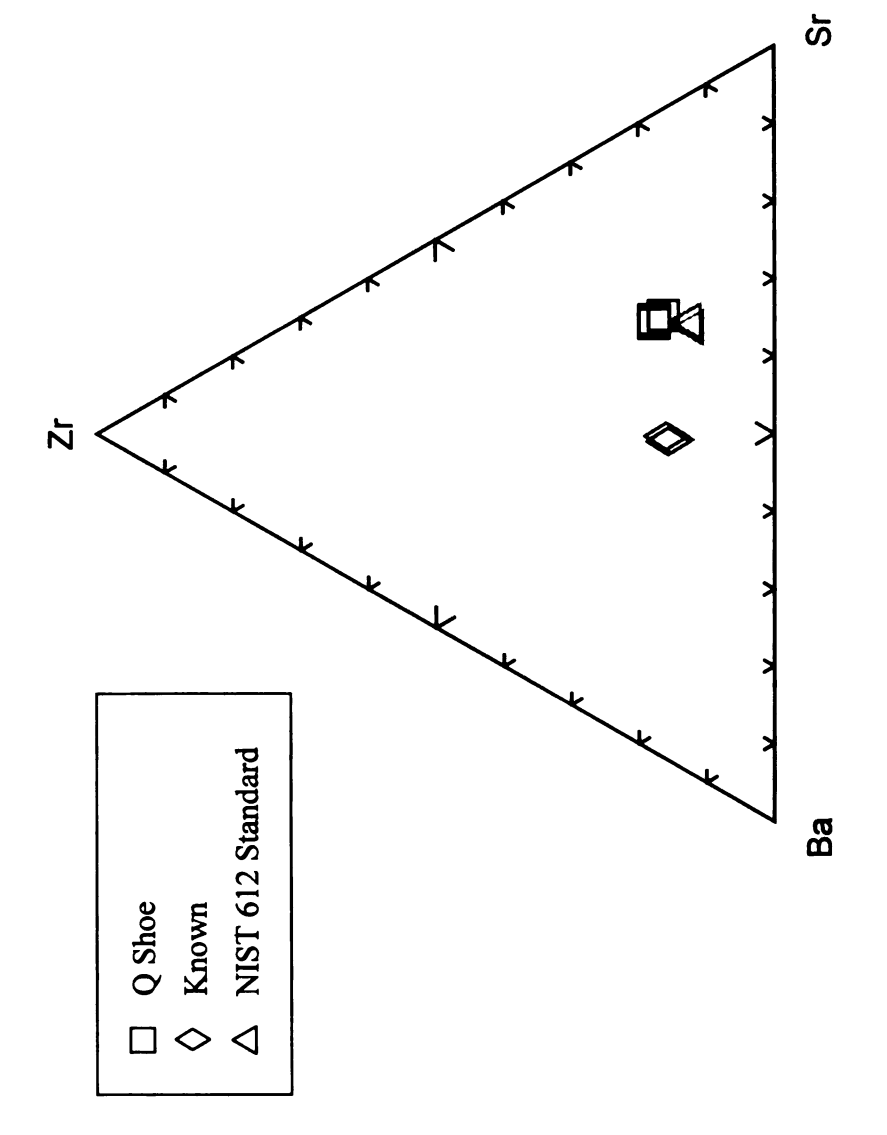
A 19 year-old resident of Dundee Village, Michigan, was accused of breaking a storefront window to gain access into a local convenience store. Two samples were submitted for analysis: one known glass fragment taken from the window frame at the point of entry and one questioned glass fragment taken from the toe area of the suspect's shoe. As in the previous examples, the questioned fragment, known fragment, and NIST 612 were ablated three times each. In this case, the questioned and known fragments were easily discriminated (Figure 12) and it was concluded the fragments did not share a common origin.

CONCLUSIONS AND FUTURE WORK

With the benefits of efficient analyses and essentially no sample preparation, LA-ICP-MS is an ideally suited for the discrimination of glass fragments. As an additional step in traditional analytical schemes involving measurement of refractive



fragment from the front porch and the known fragment from the south window could hammer handle is easily excluded as coming from the same source as the other two have originated from the same source. Note that the questioned fragment from the Figure 11. Plot showing one of the diagrams used to conclude that the questioned fragments. Again, each sample was analyzed three times.



window did not originate from the same source. As in previous cases, each sample was fragment from the suspect's shoe and the known fragment from the convenience store Figure 12. Plot showing one of the diagrams used to conclude that the questioned analyzed three times.

index, trace elemental analyses can help reduce Type II errors (or false inclusions) and improve the associative value of comparisons when samples cannot be discriminated. The range of refractive index values has become increasingly small in float glasses since about the early 1960's (Koons and Buscaglia, 2001, and references therein). However, the class size is significantly smaller for trace element composition of glasses, as demonstrated by the shrinking number of indistinguishable pairs of unknowns for a given sample suite when using chemical composition in addition to refractive index (Trejos et al., 2003; Duckworth et al., 2002).

There are several goals for maximizing the discriminatory and associative power of LA-ICP-MS glass comparisons by this method. The first is the general aim of all LA applications: improve the efficiency of sample ablation and delivery of the sample to the plasma. It has been demonstrated that newer laser ablation systems can improve laser-sample coupling, and therefore analytical precision (e.g. CETAC LSX-200® vs. LSX-500®, Trejos and Almirall, 2004). Variables such as crater shape, carrier gas types, mixture ratios, and flow rates have also been studied to improve performance (Russo et al, 2002, and references therein). As forensic glass samples are often microscopic, these parameters must often be optimized for the smallest spot size possible to obtain the most information from the sample.

For relatively short ablation times, the precision of an analysis decreases with a smaller amount of sample delivered to the ICP-MS (i.e. smaller spot size). Similarly, for the same amount of material, precision will decrease with a longer list of elements in the menu, as less time is spent scanning for any given mass-to-charge ratio (m/z). Therefore, the selection of discriminatory elements is particularly important for comparisons.

Maximizing the number of abundant elements in glasses while ensuring adequate dwell time for each element is a second goal for improving the technique. For example, the menu of six elements in the present work (⁸⁸Sr, ⁸⁹Y, ⁹⁰Zr, ¹³⁸Ba, ¹³⁹La, and ¹⁴⁰Ce) is currently being modified to include three additional, highly discriminatory isotopes (⁴⁶Ti, ⁵⁵Mn, ¹⁷⁷Hf, ²⁰⁸Pb) based partly on the work of Trejos and Almirall (2004) and Tejos et al. (2003).

In addition to demonstrating the wide range of trace element ratios observed in various float glass fragments, this study demonstrates the usefulness of LA-ICP-MS analysis in routine casework. Glass fragments have been shown to be homogeneous with respect to trace element composition, and within the precision of the technique. Although the cost of operation and maintenance has been cited as a drawback for LA-ICP-MS, the lack of sample preparation and short analysis time (even with replicates) compensates for the expense. The method is designed to be an efficient comparative tool for the forensic analyst, and by no means are the data used to quantitatively compare samples using robust statistical tests. The graphical technique of ratio comparisons is exactly that: a demonstrably precise semi-quantitative comparative tool.

REFERENCES

- Aeschliman, D.B., Bajic, S.J., Baldwin, D.P., and Houk, R.S., Multivariate pattern matching of trace elements in solids by laser ablation inductively coupled plasmamass spectrometry: source attribution and preliminary diagnosis of fractionation, *Analytical Chemistry*, 2004, 76: 3119-3125.
- Almirall, J., Elemental analysis of glass fragments, in Forensic Examination of Glass and Paint: Analysis and Interpretation, Caddy, B., ed., Taylor and Francis, 2001: 65-83.
- Becker, S., Chemometric classification of float glass and new developments in the use of laser ablation-ICP-MS in the field of glass analysis, Abstracts of the Second European Academy of Forensic Sciences Meeting, 2000.
- Curran, J.M., Triggs, C.M., Almirall, J.R., Buckleton, J.S., and Walsh, K., The interpretation of elemental composition measurements from forensic glass evidence: I, Science & Justice, 1997a, 241-244.
- Curran, J.M., Triggs, C.M., Almirall, J.R., Buckleton, J.S., and Walsh, K., The interpretation of elemental composition measurements from forensic glass evidence: II, *Science & Justice*, 1997b, 245-249.
- Duckworth, D.C., Morton, S.J., Bayne, C.K., Montero, S., Koons, R.D., and Almirall, J.R., Forensic glass analysis by ICP-MS: A multi-element assessment of discriminating power via analysis of variance and pair-wise comparisons, *Journal of Analytical and Atomic Spectrometry*, 2002, 17: 662-668.
- Duckworth, D.C., Bayne, C.K., Morton, S., and Almirall, J.R., Analysis of variance in forensic glass analysis by ICP-MS: variance within the method, *Journal of Analytical and Atomic Spectrometry*, 2000, 15: 821-828.
- Durrant, S.F., Laser ablation inductively coupled plasma mass spectrometry: achievements, problems, prospects, *Journal of Analytical and Atomic Spectrometry*, 1999, 14: 1385-1403.
- Hickman, D.A., Glass types identified by chemical analysis, Forensic Science International, 1987, 33: 23-46.
- Koons, R.D., and Buscaglia, J., Interpretation of glass composition measurements: The effects of match criteria on discrimination capability, *Journal of Forensic Sciences*, 2002, 47: 505-512.
- Koons, R.D., and Buscaglia, J., Distribution of refractive index values in sheet glasses, *Forensic Science Communications*, 2001, 3.

- Montero, S., Hobbs, A.L., French, T.A., and Almirall, J.R., Elemental analysis of glass fragments by ICP-MS as evidence of association: analysis of a case, *Journal of Forensic Sciences*, 2003, 48: 1-7.
- Parouchais, T., Warner, I.M., Palmer, L.T., and Kobus, H., The analysis of small glass fragments using inductively coupled plasma mass spectrometry, *Journal of Forensic Sciences*, 1996, 41: 351-360.
- Russo, R.E., Mao, X., Liu, H., Gonzales, J., and Mao, S.S., Laser ablation in analytical chemistry a review, *Talanta*, 2002, 57: 425-451.
- Suzuki, Y., Sugita, R., Suzuki, S., and Maruma, Y., Forensic discrimination of bottle glass by refractive index measurement and analysis of trace elements with ICP-MS, *Analytical Sciences*, 2000, 16: 1195-1198.
- Szymanski, D., Patino, L., Bommarito, C., and Siegel, J., Trace element profiles of float glass fragments determined by laser ablation inductively coupled plasma mass spectrometry (LA-ICP-MS), Abstracts of the 56th Annual Meeting of the American Academy of Forensic Sciences, 2004, Dallas, TX.
- Szymanski, D., Patino, L., Bommarito, C., and Siegel, J., Use of laser ablation inductively coupled plasma mass spectrometry (LA-ICP-MS) for float glass fragment discrimination by elemental analysis: preliminary results, Abstracts of the 32nd Annual Meeting of Midwestern Association of Forensic Scientists, 2003, Columbus, OH.
- Trejos, T. and Almirall, J.R., Effect of fractionation on the forensic elemental analysis of glass using laser ablation inductively coupled plasma mass spectrometry, *Analytical Chemistry*, 2004, 76: 1236-1242.
- Trejos, T., Montero, S., Almirall, J.R., Analysis and comparison of glass fragments by laser ablation inductively coupled plasma mass spectrometry (LA-ICP-MS) and ICP-MS, *Analytical and Bioanalytical Chemistry*, 2003, 376:1255-1264.
- Watling, R.J., Novel application of laser ablation inductively coupled plasma mass spectrometry in forensic science and forensic archaeology, *Spectroscopy*, 1999, 14: 16-34.
- Watling, R.J., Lynch, B.F., and Herring, D., Use of laser ablation inductively coupled plasma mass spectrometry for fingerprinting crime scene evidence, *Journal of Analytical and Atomic Spectrometry*, 1997, 12: 195-203.

